Uses of Superconductivity in Particle Accelerators

R. H. Siemann
Stanford Linear Accelerator Center
Stanford, CA 94309

1. INTRODUCTION

Progress in science is critically dependent on advances of its instruments. Accelerators are one of the principal instruments of high energy physics, and particle physics discoveries are often preceded by accelerator developments. Examples are the discovery of the τ and one of the two independent discoveries of the J/ψ that followed the construction of SPEAR, the first modern e^+e^- storage ring, and the discovery of the Z and W's following the invention of stochastic cooling at CERN. Accelerators are pushing the limits of technology, and, therefore, technological progress can lead to particle physics discoveries through their impact on accelerators.

These lectures are devoted to superconductivity. Superconductivity is a fascinating physics topic by itself,* but these lectures concentrate on it as a technology that is becoming increasingly important to high energy physics. The theme of this year's SLAC Summer Institute was lepton-hadron scattering. HERA, the next major lepton-hadron scattering facility, depends on superconductivity for the proton ring magnets and electron ring RF (Radio Frequency) accelerating system. That connects these lectures to the others at the Summer Institute.

Superconducting magnets and RF are used in high energy physics, and they affect performance and economy. The following examples illustrate this.

Superconducting Magnets & Hadron Rings: Superconducting magnets are central elements of any modern, high energy proton synchrotron or storage ring. The bending radius of a particle is $\rho = p/eB$ where p, e and B are the momentum, charge and magnetic field. Conventional magnets (an iron yoke with current carried in copper conductors) can reach $B \sim 2T$ before the iron saturates while superconducting magnets can reach up to three or four times higher field. We wouldn't even be thinking about HERA, the LHC and the SSC without superconducting magnets. They would be too large or the center-of-mass energy too low. In addition, they would be too expensive to operate. The Fermilab fixed target programs offer a good illustration. The old 400 GeV fixed target program based on the Main Ring used 83 MW of AC power while the present Tevatron based 800 GeV fixed target program uses only 44 MW[1].

---

* Nobel prizes for work related to superconductivity include H. K. Onnes for the liquefaction of He and his investigations of materials at low temperatures (1913), J. Bardeen, L. N. Cooper, and J. R. Schrieffer for the development of the theory of superconductivity (1972), I. Giaever and B. D. Josephson for investigations of tunneling (1973), and K A. Müller and J. G. Bednorz for the discovery of high-T_C superconductors (1987).

Superconducting Magnets & Electron Colliders: Superconducting quadrupoles are used as focusing elements at the interaction regions of LEP, the SLC, and are proposed for some B-Factories. They have high fields that give strong focusing while immersed in the solenoidal field of a detector.

There is a potential economic impact of superconducting magnets for linear colliders. Several laboratories including SLAC are developing X-band (~3 cm wavelength) klystrons as RF power sources. The present SLAC design gives 100 MW of peak RF power with a 9.6×10^{-5} duty cycle for an average RF power of 9.6 kW. That requires 22 kW of average klystron beam power, so the conversion efficiency is 44%. However, the klystron beam must be focused, and conventional magnets for that require about 25 kW[2]. That would reduce the efficiency to about 20%. Superconducting or permanent magnets are needed for reasonable efficiency.

Superconducting RF & Electron Storage Rings: An electron in a storage ring loses energy to synchrotron radiation. The energy loss per turn is $U_0 \propto p^4/\rho$. The RF system must make up that energy loss and have a peak voltage per turn $V_{PK} > U_0/e$. When LEP operates at 55 GeV, the top energy of LEP I, U_0 = 260 MeV and the synchrotron radiation power is $P_{SR}(= I_{BEAM}U_0/e)$ = 1.6 MW[3]. LEP I has an RF system of copper cavities. With that system there are ~12 MW of cavity wall losses at the required V_{PK}. That's the cost of producing the voltage - approximately 90% of the RF power just heats the walls of the RF cavities.

At 95 GeV per beam, above the W^+W^- threshold, U_0 = 2300 MeV and P_{SR} = 14 MW. It isn't feasible to generate this high a voltage with a copper RF system that fits in the LEP tunnel, and, even if that weren't the case, such a system would be prohibitively expensive. A superconducting RF cavity (operating with 100% duty cycle as needed for a storage ring) has a higher accelerating gradient than a copper RF cavity and wall losses that are almost zero. LEP II with superconducting RF will have an energy above the W-pair threshold while using the same amount of RF power as LEP I. Superconducting RF promises higher luminosity at the Z, also. Once the superconducting RF system is installed the power now needed to generate V_{PK} can be used to raise the beam current and luminosity instead.

Beams generate electromagnetic fields as they pass through RF cavities. These "wake fields" have bad effects including causing instabilities. Superconducting RF is being proposed for some B-Factories because the higher accelerating gradient allows wake fields to be reduced by reducing the number of RF cavities.

Superconducting Linear Accelerators: Coincidence experiments benefit from a high duty cycle because that reduces accidentals. CEBAF is a high duty cycle, 6 GeV, electron linac designed primarily for coincidence electron scattering experiments. The original concept was for a room temperature, pulsed linac that injected into a stretcher ring; the beam was to be extracted slowly from the stretcher ring to get a high duty cycle[4]. As a result of technical evaluations a superconducting RF linac that can run with a 100% duty cycle is being built instead[5].

The most speculative use of superconducting RF is for high energy linear colliders. There is a trade-off between the efficiency of superconducting RF and the higher acceleration gradient of pulsed, room temperature RF.

These examples illustrate the importance of superconductivity to particle physics. The rest of these lecture notes expand on these ideas and discuss the ways that the unique features of superconductivity affect performance and possibilities.

2. SUPERCONDUCTING MAGNETS

2.1 Basics of Superconductivity

Superconductivity is explained by the Bardeen, Cooper and Schrieffer (BCS) theory where there is an attractive interaction, mediated by the crystal lattice, between pairs of electrons, "Cooper pairs", that have spin equal to zero and many of the attributes of bosons[6]. It is one of the most important phenomena of physics and is covered in most solid state physics text books. The goal of this section is to present some of the phenomenology of DC superconductivity that is important for accelerator magnets. Kittel's book *Introduction to Solid State Physics* is followed closely, paraphrased, and quoted in this section[7].

The DC (constant current and voltage) electrical resistance of a superconductor in the superconducting state equals zero. The magnetic properties are unique, and they are different from those of a perfect conductor. The "Meissner effect" is the exclusion of magnetic field from a superconductor. It is different from having zero resistance because magnetic field is expelled when the temperature of a sample in a constant magnetic field is reduced such that the material makes a transition from a normal to a superconducting state.

Consider a long, thin circular rod of superconductor immersed in a magnetic field $\mathbf{B} = \mathbf{B}_A$ as shown in Figure 1. Inside the superconductor the magnetization, $\mathbf{M}$, opposes $\mathbf{B}_A$ so that $\mathbf{B} = \mathbf{B}_A + \mu_0\mathbf{M} = 0$. The magnetization is produced by currents circulating around the outside of the rod. There are two types of superconductors, type I and type II, that have different dependences of M on B_A. These are shown in Figure 2. The magnetization of a type I superconductor is directly proportional to B_A up to a critical field B_{C1}, and above B_{C1} the material is normal. The critical field is a function of temperature, $B_{C1}(T)$, and at the critical temperature, T_C, $B_{C1}(T_C) = 0$. Excluding flux increases the magnetic field and its associated energy outside the superconductor. Despite this it is energetically favorable to exclude flux because of the lower entropy and the stabilization free energy of the superconducting state. The free energy density is

$$\Delta F = -\int \mathbf{M}\cdot d\mathbf{B}_A = B_{C1}^2/2\mu_0 \quad . \tag{1}$$

The magnetization of a type II superconductor is also directly proportional to B_A up to B_{C1}; there is complete magnetic field exclusion for $B_A \le B_{C1}$. When B_A exceeds B_{C1} flux penetrates into a type II superconductor in normal regions surrounded by superconducting ones (Figure 3). The material remains a perfect electrical conductor until $B_A \ge B_{C2}$. There it makes a transition from a state with zero electrical resistance to a normal state with finite resistance. Both B_{C1} and B_{C2} depend on temperature. The stabilization free energy density,

$$\Delta F = -\int \mathbf{M}\cdot d\mathbf{B}_A = B_C^2/2\mu_0, \tag{2}$$

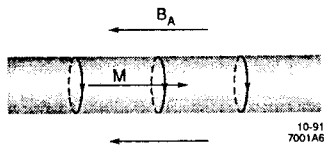

Figure 1: A rod of superconductor immersed in a magnetic field.

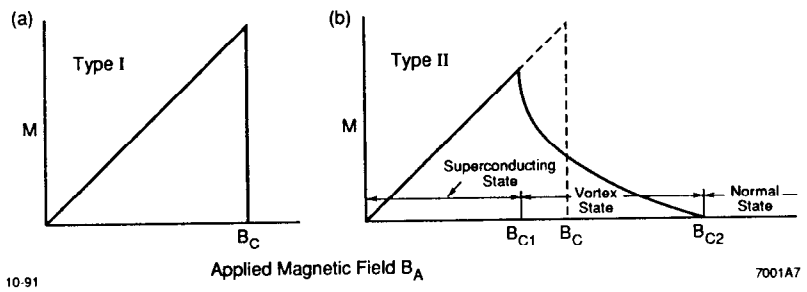

Figure 2: Magnetization vs applied magnetic field for a) type I and b) type II superconductors[7].

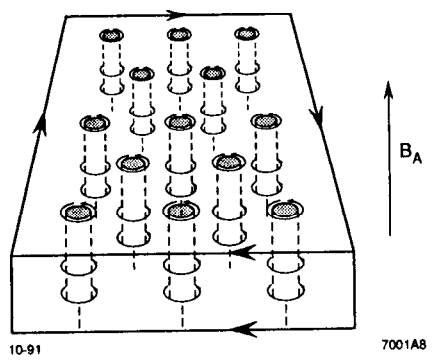

Figure 3: The vortex state showing normal cores and circulating current vortices[8].

gives the thermodynamic critical field B_C. It is

$$B_c = \sqrt{B_{C1}B_{C2}} \quad . \tag{3}$$

The upper critical field, B_{C2}, is substantially greater than B_C, and that is the reason type II superconductors are used in superconducting magnets.

There are three important lengths. The first one is the "London penetration depth", λ, which is the decay length of the magnetic field at the surface of the superconductor

$$B = B_A \exp(-r/\lambda) \quad . \tag{4}$$

Typically, $\lambda \sim 500$ Å for a type I superconductor. The second important length is the coherence length, ξ. It is the characteristic distance in the order parameter that gives the concentration of Cooper pairs, and the Cooper pair density cannot change drastically over ξ in a spatially varying magnetic field. The penetration depth and coherence length depend on Λ, the mean-free-path of electrons in the normal state; $\xi \sim \Lambda^{1/2}$, $\lambda \sim \Lambda^{-1/2}$, and $\kappa \equiv \lambda/\xi \sim 1/\Lambda$. The proportionality constants depend on properties of the material including the density of Cooper pairs, the energy gap of the superconducting state, and the electron velocity at the Fermi surface.

Type I superconductors are materials with a long mean-free-path in the normal state and a coherence length that is much greater than the penetration depth ($\xi \gg \lambda$ and $\kappa \ll 1$). Type II superconductors have a short mean-free-path in the normal state, a coherence length that is much shorter than the penetration depth ($\xi \ll \lambda$), and $\kappa \gg 1$. A type I superconductor can be changed to type II by adding a modest amount of alloying material to reduce the mean-free-path without affecting other properties such as T_C.

There is a vortex state in type II superconductors between B_{C1} and B_{C2}. The magnetic field penetrates in quantized units of magnetic flux called fluxoids

$$\Phi_0 = \frac{h}{2e} = 2.068\times10^{-15}\,\text{T-m}^2 \tag{5}$$

in normal regions that are surrounded by superconducting regions (Figure 3). At B_{C2} the fluxoids are packed together as tightly as possible consistent with there being superconducting regions between them. When a type II superconductor carries transport current, as it must in a superconducting magnet, the transport current and the magnetic field interact and produce forces on each other. The Lorentz force per unit length on a fluxoid is[8]

$$F_L = J\Phi_0 \tag{6}$$

where J is the average current density and the angle between the field and the current is assumed to be 90°. If there were no force to counteract this force the fluxoids would move thereby inducing a voltage and, effectively, a resistance. There must be a force counteracting the Lorentz force. This "pinning force" comes from imperfections in the

material that fix the location of some fluxoids. The remainder are pinned because of the rigidity of the fluxoid lattice. The critical transport current density J_C is reached when the Lorentz force equals the average flux pinning force, F_P,

$$J_c \Phi_0 = F_P \quad . \tag{7}$$

A good superconductor for use in a magnet has a large number of imperfections that produce a large flux pinning force.

2.2 Current Sheet Magnets

The field profile of conventional magnets is usually dominated by the shape and location of the iron poles which are magnetostatic equipotentials. The precise locations of the current carrying conductors are not critical. In contrast the field profile of most superconducting magnets is determined by the current distribution.*

The fields in a superconducting magnet can be understood by starting with a current flowing in an infinitely long cylindrical shell of radius a,

$$J_z(r',\phi') = I_m \delta(r'-a)\cos(m\phi') \quad . \tag{8}$$

This is one component of a Fourier analysis. The vector potential is

$$A_Z(r,\phi) = \frac{\mu_0}{4\pi}\int \frac{J_z(\mathbf{r}')}{|\mathbf{r}'-\mathbf{r}|}\, d^3r' \quad . \tag{9}$$

Using the Green's function for Poisson's equation in polar coordinates[10]

$$A_z(r,\phi) = \frac{\mu_0 I_m}{2m}\left[\frac{r}{a}\right]^m \cos(m\phi) \quad . \tag{10}$$

This gives

$$B_r(r,\phi) = -\frac{\mu_0 I_m}{2a}\left[\frac{r}{a}\right]^{m-1} \sin(m\phi) \quad , \tag{11}$$

and

$$B_\phi(r,\phi) = -\frac{\mu_0 I_m}{2a}\left[\frac{r}{a}\right]^{m-1} \cos(m\phi) \quad . \tag{12}$$

Different values of m produce different field configurations. A dipole magnet is produced by a current distribution with m = 1. In that case

$$B_r = -\frac{\mu_0 I_1}{2a}\sin(\phi) \;;\; B_\phi = -\frac{\mu_0 I_1}{2a}\cos(\phi) \quad . \tag{13}$$

* "Superferric" magnets are in between[9]. Iron is used to help shape the field that is produced by superconducting current carriers. They have not found wide use in high energy physics.

The magnitude of $|\mathbf{B}|$ is independent of r and ϕ. Transforming to Cartesian coordinates

$$\begin{aligned} B_x &= B_r\cos(\phi) - B_\phi \sin(\phi) = 0 \;; \\ B_y &= B_r\sin(\phi) + B_\phi\cos(\phi) = -\frac{\mu_0 I_1}{2a} \quad . \end{aligned} \tag{14}$$

The field is a *uniform* field pointing in the y direction. Dipoles are used to bend particles, and they are the main magnetic elements of any storage ring or synchrotron.

A quadrupole magnet is produced by a current distribution with m = 2. It has $|\mathbf{B}| \sim r/a$ independent of ϕ. The fields in Cartesian coordinates are

$$B_x = -\frac{\mu_0 I_2}{2a^2}\, y \quad \text{and} \quad B_y = -\frac{\mu_0 I_2}{2a^2}\, x \quad . \tag{15}$$

These are the *focusing* magnets that keep the beam confined to the desired trajectory.

Sextupole magnets have m = 3; they are also used in accelerators to correct the momentum dependent focusing of quadrupoles. Multipolarities higher than m = 3 are rarely used on purpose, but they appear as the result of approximations to the ideal current distribution (see the next section), errors, and persistent currents. The harmful effects of "non-linear" multipoles, m = 3 and higher, are discussed in Section 2.5.

2.3 Real Magnets*

It is impossible to wind a coil with only one Fourier component; the coil cross section would be too complicated. Magnets are made with coils that are relatively easy to wind and give an adequate approximation to the desired current distribution. Dipoles are discussed in this section to illustrate this.

The easiest possibility is to wind coils with a uniform cross section extending over some angle Φ' as illustrated in Figure 4. A coil with this symmetry has only odd Fourier components, m = 1,3,5,... . Those Fourier components are $I_m \sim \sin(m\Phi')$. The sextupole component of the current distribution equals zero if $\Phi' = 60°$, and in that case the magnet has m = 1,5,7,11,... . While this coil geometry is simple, the decapole (m = 5) component is unacceptably large. At r = a/2, a reasonable goal for the extent of the useful field, $|B_5/B_1| = 1.3\times10^{-2}$.

Coils are built out of conductors with a keystone cross section. Staying with a one layer coil and reducing the higher multipoles is possible with spacers to reduce the current where desired. The RHIC dipoles have a single layer coil (Figure 5) that approximates $\cos\phi'$ in this way. Dipoles with single layer coils have limited field because of considerations of *i)* coil winding and the stiffness of the conductor, *ii)* the maximum keystone possible, and *iii)* the economical use of superconductor[12]. High field magnets are built with two layer coils. The angles of the inner and outer coils

* The general approach of this section as well as many of the specific examples come from ref. [11].

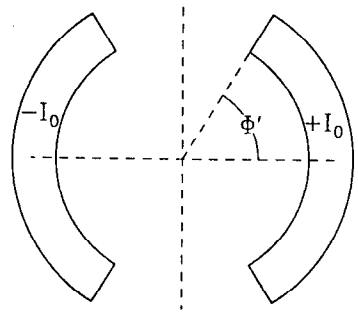

Figure 4: A simple dipole coil configuration.

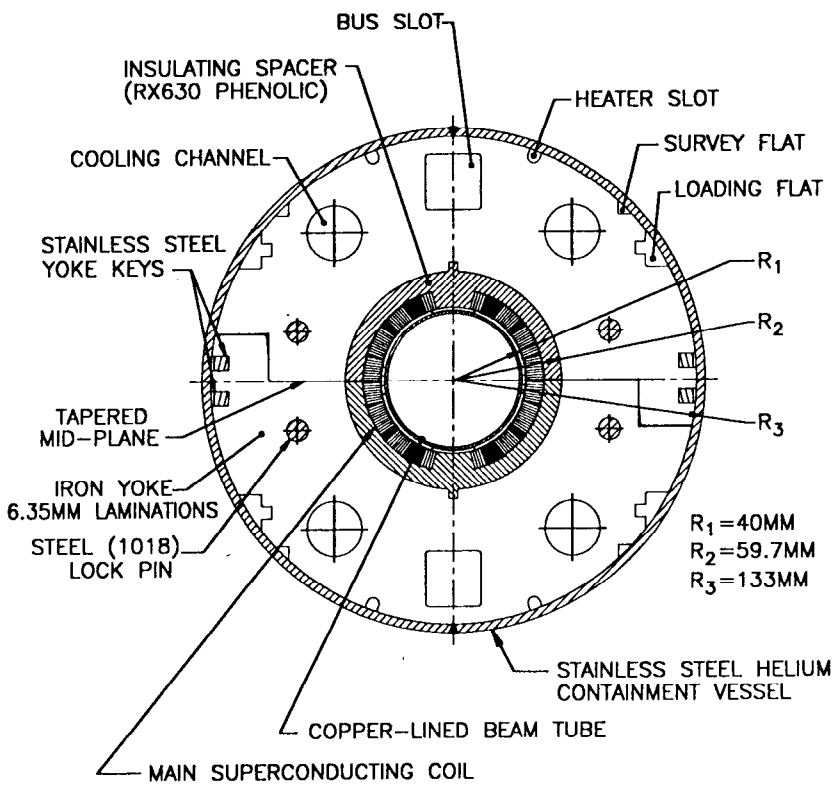

Figure 5: The RHIC dipole (figure courtesy of S. Ozaki).

can be chosen to cancel the sextupole and decapole leaving m = 7 as the lowest unwanted multipole. That was done for the Tevatron dipole shown in Figure 6; the field quality was satisfactory in that case because of the high ratio of injection-to-storage energies at the Tevatron.* Double layer coils with wedges are used in HERA, the SSC, and the LHC where high fields and good field quality are both needed (see Figure 7).

The simple coil in Figure 4 can be used to estimate conductor placement tolerances. An angular placement error leads to a relative sextupole field

$$b_3 \equiv \frac{|\mathbf{B}_3|}{|\mathbf{B}_1|} = \frac{1}{3}\left[\frac{r}{a}\right]^2 \frac{\sin(3\Phi'+3\delta\Phi')}{\sin(\Phi'+\delta\Phi')}\Bigg|_{60^\circ} \simeq -\,0.39\left[\frac{r}{a}\right]^2 \delta\Phi' \,. \tag{16}$$

A typical specification is $|b_3| < 1\times10^{-4}$ at r/a = 1/2. This leads to $|\delta\Phi'| < 1$ mrad, and for a coil such as that of the SSC with the conductor about 3 cm from the center of the bore, the position tolerance is ~ 30 μm. Tooling with this level of tolerance is used for winding and baking the coils once they are epoxy impregnated, and a collar assembly made from precisely stamped laminations holds the coil in place to these tolerances. Figure 8 illustrates this.

Achieving this precision is just one aspect of the impressive engineering that has gone into building superconducting magnets. Besides coil placement, considerations of magnetic forces, effects of iron on field quality, shrinkage during cooldown, coil ends, quench protection, training, low heat loss cryostats, etc are all important. The cryogenic systems of large hadron rings are massive installations, and the high efficiency refrigerators that can operate in the range of conditions encountered in a superconducting accelerator are fascinating. These subjects are too much to be covered in an article such as this aimed for a readership of particle physicists, and there are well written reviews about magnets[11,13,14] and cryogenic systems[15] available.

Because of a favorable combination of magnetic properties and ease of working (bending, winding, shaping), NbTi is usually used in accelerator magnets. Nb_3Sn has a higher critical temperature and critical field, T_C = 18.1 K and B_{C2} = 22.5 T vs 9.5 K and 14.5 T for NbTi, but it is brittle and extremely difficult to handle. NbTi performance is characterized by a three-dimensional critical surface (Figure 9) with temperature, magnetic field and current density as the axes; NbTi is superconducting within this surface. The critical temperature, T_C, and B_{C2} are indicated in this figure as the intersections of the projection in the J = 0 plane with the T and B axes. By convention the "critical current" of a conductor is usually quoted as the critical current at T = 4.2 K (the boiling point of ^{4}He) and B = 5 T.

The "Rutherford Cable"[16] that is used in high energy accelerators is shown in Figure 10. It has a keystone shape with a small keystone angle ~ 1° - 2°. The cable consists of strands that are about 1 mm in diameter and twisted to form a gentle spiral to minimize the magnetic flux that couples strands inductively. The strands

* At the Tevatron E_{INJ} = 150 GeV and E_{STORE} = 1 TeV.

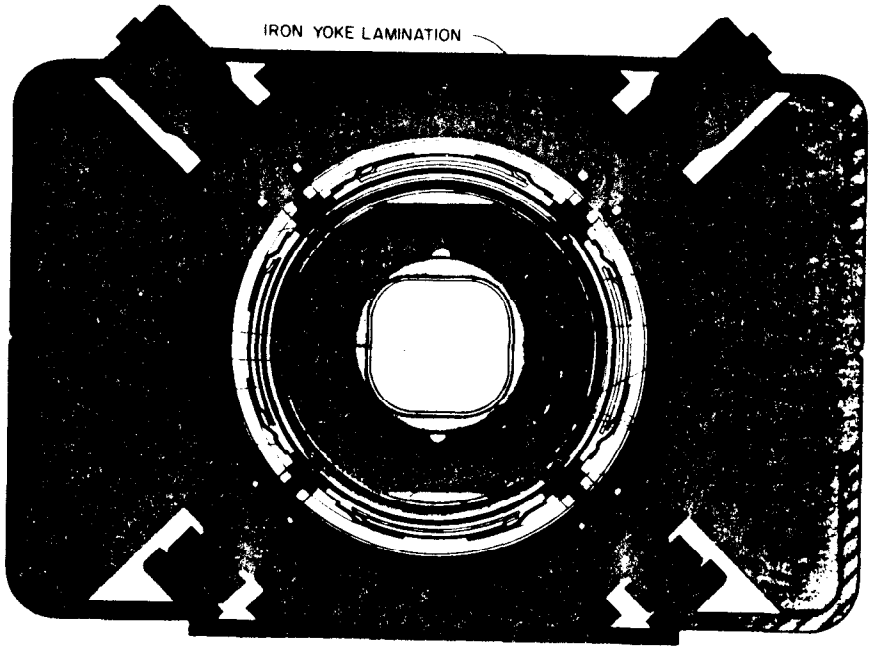

Figure 6: The Tevatron dipole (figure courtesy of R. Rubenstein).

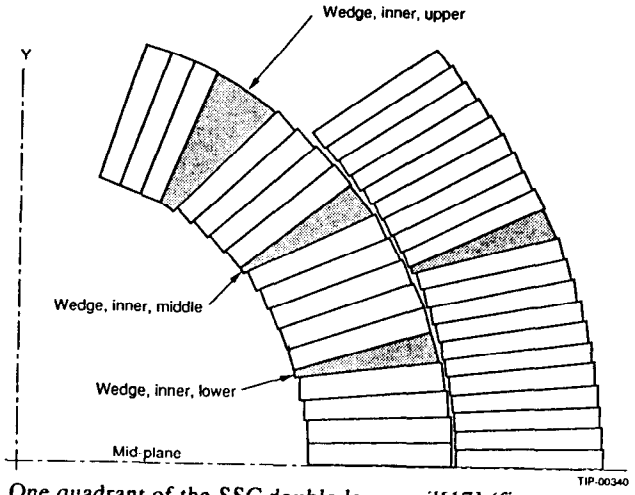

Figure 7: One quadrant of the SSC double layer coil[17] (figure courtesy of N. Baggett).

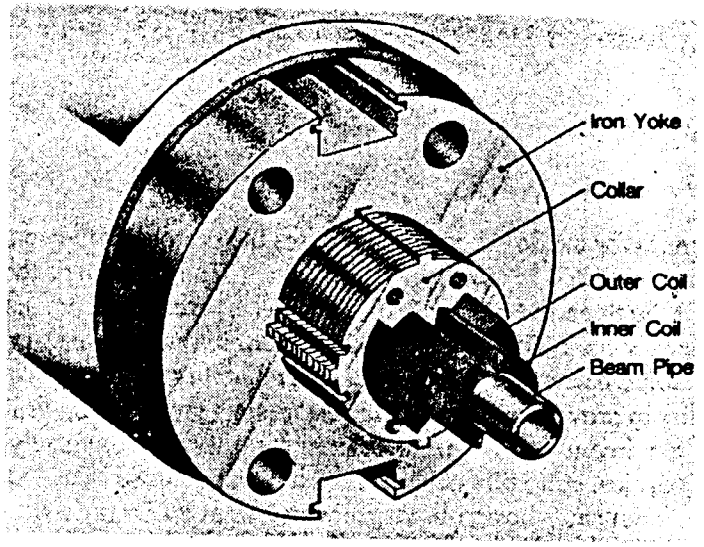

Figure 8: Schematic of major dipole components[17] (figure courtesy of N. Baggett).

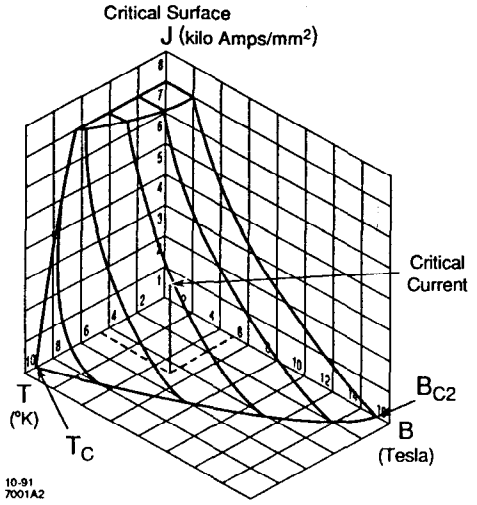

Figure 9: Critical surface for NbTi[13].

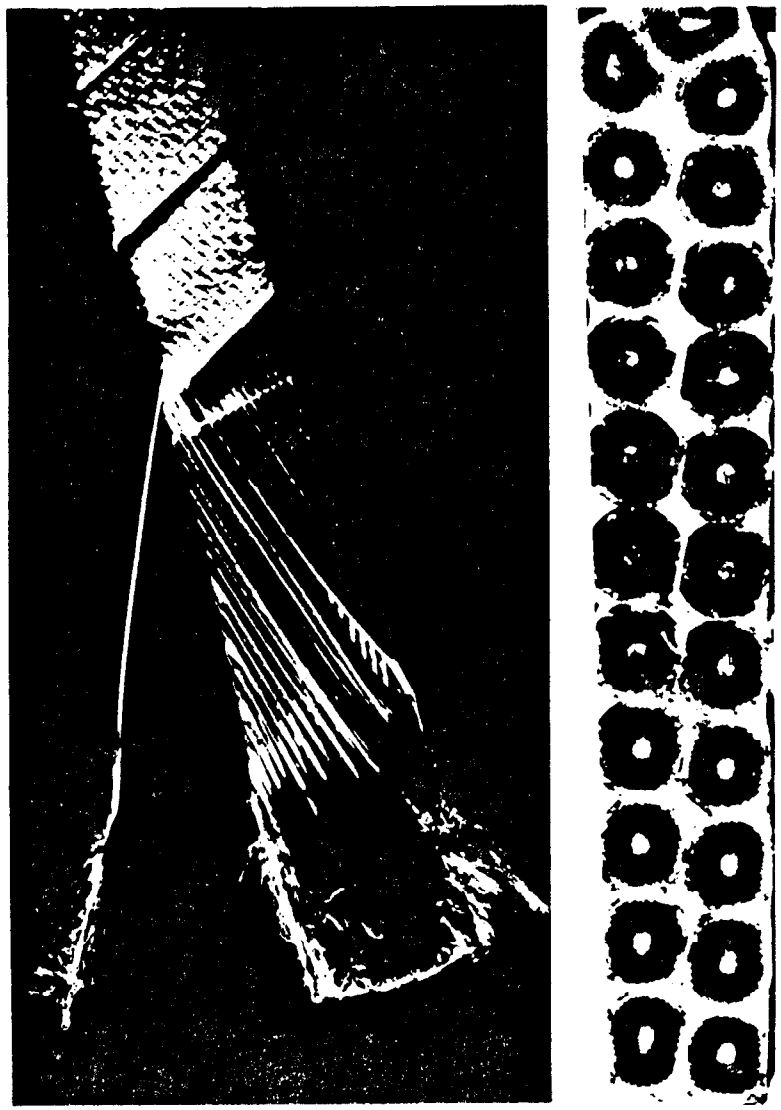

Figure 10: Enlargements of the SSC superconducting cable[18] (photo courtesy of N. Baggett).

themselves are a matrix of NbTi conductors with copper between them. They are made by inserting NbTi rods several mm in diameter into holes at the centers of hexagonally shaped copper rods. These rods are packed into an extrusion billet and then extruded and drawn at high temperatures until the diameter of the NbTi rods is reduced to ~ 5 μm. Figure 11 is a microphotograph of a superconducting strand.

The critical current is controlled by extrinsic factors such as the uniformity of the filaments that can be produced during the drawing process and metallurgy of NbTi in a copper matrix and intrinsic factors such as the flux pinning force. The development of this cable and conductor design and the improvement of the critical current over the last decade (Figure 12) are important advances in accelerator technology and major contributions to high energy physics.

2.4 Persistent Currents

Currents flow in a superconducting filament to exclude flux. These currents are called "persistent currents" because until about five years ago accelerator builders thought they would flow forever like the persistent currents in type I superconductors. They cause non-linear fields that have important implications for the beams in superconducting accelerator rings. They produce an aperture, and any particles outside that aperture are lost. This aperture isn't a "physical aperture" produced by solid obstacles such as a beam-pipe; it is a "dynamic aperture" produced by magnetic field non-linearities.

Figure 13 shows an infinitely long wire of radius R immersed in a uniform applied magnetic field, $\mathbf{B}_A = B_A\mathbf{j}$. Consider the behavior as B_A is raised slowly. When $B_A < B_{C1}/2$, magnetic flux is excluded from the wire by a surface current

$$J_z(r',\phi') = \frac{2RB_A}{\mu_0}\,\delta(r'-R)\cos(\phi') \quad . \tag{17}$$

The total magnetic field outside the wire ($r \geq R$) is

$$\mathbf{B} = B_A\left\{\mathbf{j}\left[1+\frac{R^2}{r^2}\cos(2\phi)\right]-\mathbf{i}\left[\frac{R^2}{r^2}\sin(2\phi)\right]\right\} \quad . \tag{18}$$

The field is largest at $\phi = 0, \pi$ where $B = 2B_A$. When the applied field is raised until $B_A > B_{C1}/2$, the field penetrates the wire in those two regions first, and a bipolar current with density $J_C(B,T)$, the critical current at the local field B and temperature T, flows[16]. In addition, surface currents flow where the flux hasn't penetrated to produce a field free region at the center of the wire.

As the applied field is raised further, flux penetrates the entire wire, and half the wire has a current with density J_C in the +z direction while the other half has current with density J_C in the -z direction, see Figure 14. This is a magnetic dipole with a magnetization, the magnetic moment per unit volume, given by

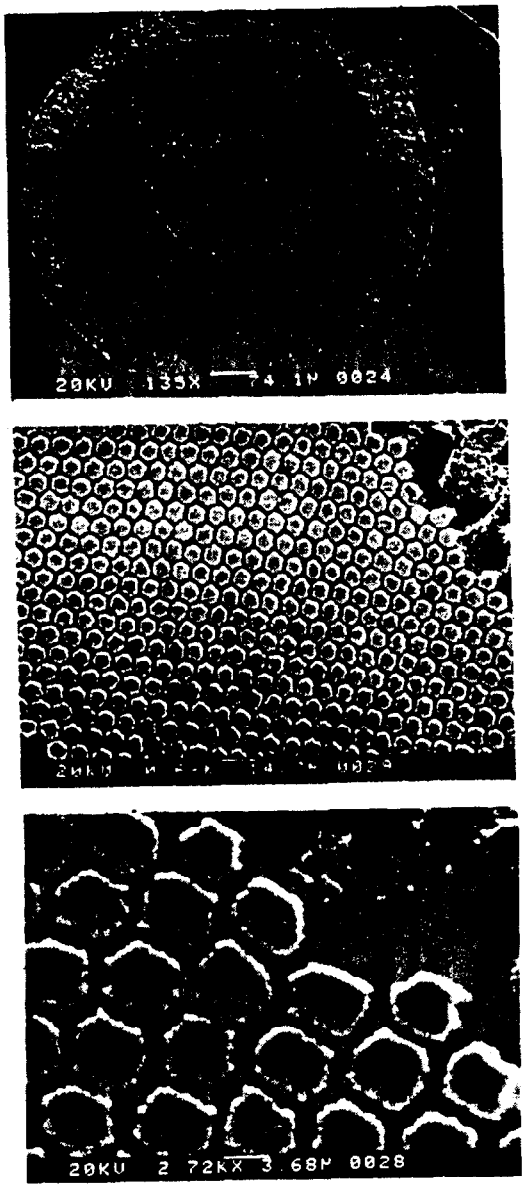

Figure 11: Microphotograph of a superconducting strand[17] (photo courtesy of N. Baggett).

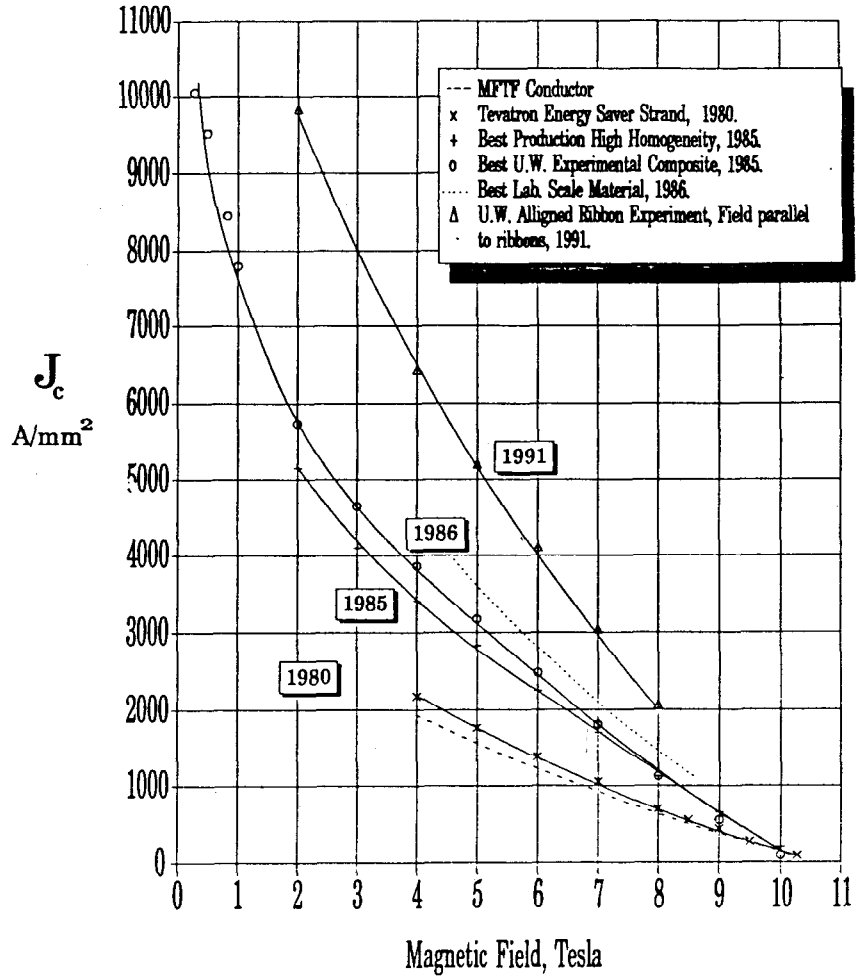

Figure 12: Progress in raising the critical current of NbTi[19] (figure courtesy of P. J. Lee and D. Larbalestier).

$$\mathbf{M} = -\frac{4RJ_C}{3\pi}\,\mathbf{j}\ . \tag{19}$$

The applied field can be raised still further as long as the field in the wire remains less than B_{C2}. The magnetization is still given by eq. 19, but it falls as B increases because J_C decreases. As discussed below this magnetization produces sextupole and higher order fields in dipole magnets.

If the applied field would be decreased now, flux would be expelled from the center of the wire first leading to a complex pattern of currents flowing in the wire and hysteretic behavior of the magnetization[11]. Figure 15 shows the sextupole moment of a Tevatron dipole (normalized to the dipole field at the reference radius) and its dependence on the direction of the current ramp. The asymptotic approach to a systematic value associated with the coil geometry and the hysteresis at low currents are clear. During accelerator operations the magnets are cycled below the injection energy and then raised to the injection field so that one is always on the *rising current* branch of the hysteresis loop and the wires are fully magnetized as in Figure 14 when beam is injected.

The discussion above was for one superconducting wire - one filament in one strand in one cable of the conductor! Each filament is magnetized with a magnetic moment pointing opposite the applied magnetic field, the field from the current in all the other conductors, and each of these magnetic dipoles produces fields that can affect the beam. Integrating over the magnetization of the coil gives[20,21]

$$\mathbf{B}_M \sim J_C R \left\{ \frac{1}{a^4}\,\mathbf{B}_{\text{Sextupole}} + \frac{1}{a^6}\,\mathbf{B}_{\text{Decapole}} + \ldots \right\} \tag{20}$$

which must be added to the field produced by the transport current to get the total magnetic field. In this equation the dependence on a, the coil radius, is shown explicitly and the individual multipole fields depend on the coil geometry. The dependence on the filament radius, R, comes directly from eq. 19, and reducing R reduces these unwanted multipoles. That is the reason for making filaments as small as practical.

2.5 Effects of Non-Linear Fields

Particles in a synchrotron or storage ring are bent by the dipoles, focused by the quadrupoles and accelerated by the RF. As a first model for understanding the effects of non-linear fields ignore the bending and acceleration and consider a beam traveling in the z direction in a vector potential

$$\mathbf{A} = \mathbf{k}\,A_z(r,\phi)\ . \tag{21}$$

The Hamiltonian for this motion is

$$H = \left\{ m^2c^4 + (\mathbf{p}-e\mathbf{A})^2c^2 \right\}^{1/2}\ . \tag{22}$$

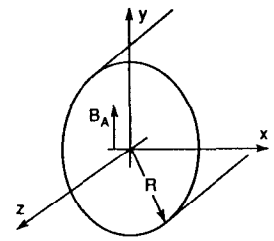

Figure 13: The coordinates used in Section 2.4

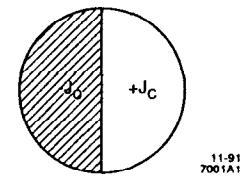

Figure 14: The magnetic dipole formed as flux penetrates the entire wire.

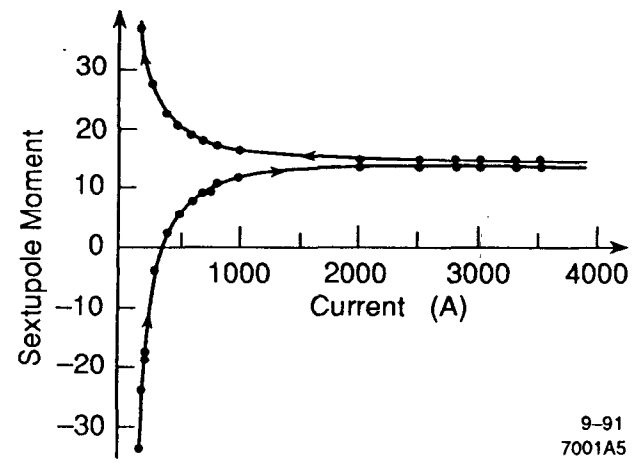

Figure 15: The sextupole moment of a Tevatron dipole[21]. The systematic value is caused by coil placement errors.

Individual particles have momentum components transverse to the z-axis (the focusing of the quadrupoles prevents the beam from blowing up), but these components are much smaller than the longitudinal momentum, $|p_z| >> |p_x|, |p_y|$. The vector potentials for the quadrupole and persistent current sextupoles are smaller still, $|p_x|, |p_y| >> |eA_z|$.* Expanding the Hamiltonian and keeping leading terms

$$H = H_0 + \frac{c^2}{H_0}\left\{\frac{p_x^2}{2} + \frac{p_y^2}{2} - eA_z p_z\right\} \tag{23}$$

where

$$H_0 = \left\{m^2c^4 + p_z^2c^2\right\}^{1/2} \tag{24}$$

is a constant and is approximately the energy of the particle. The second term in eq. 23 is the energy associated with the transverse oscillation, and it is a constant since the total energy, given by the Hamiltonian H, and H_0 are constant;

$$H_T = \frac{c^2}{H_0}\left\{\frac{p_x^2}{2} + \frac{p_y^2}{2} - eA_z p_z\right\} = \text{constant} \ . \tag{25}$$

Look at the motion in a quadrupole first. Equation 10 gives

$$A_z = \frac{\mu_0 I_2}{4a^2}(x^2 - y^2) \tag{26}$$

for a quadrupole, and

$$H_T = \frac{c^2}{H_0}\left\{\left[\frac{p_x^2}{2} - \frac{e\mu_0 I_2}{4a^2}x^2\right] + \left[\frac{p_y^2}{2} + \frac{e\mu_0 I_2}{4a^2}y^2\right]\right\} \ . \tag{27}$$

The two transverse dimensions are independent, and there is kinetic energy and potential energy in each. If $eI_2 > 0$, the potential energy in the y-direction is quadratic with positive curvature (see Figure 16) and the y-motion is stable, bounded simple harmonic oscillation. For the same sign of eI_2 the potential energy in the x-dimension is quadratic with negative curvature, and the x-coordinate grows exponentially. On the other hand if $eI_2 < 0$, the x-motion is bounded and the y-coordinate grows exponentially. Quadrupoles focus in only one dimension, and the principle of "strong focusing" or "alternating gradient focusing" is that focusing and stable bounded oscillations are possible in both transverse dimensions by alternating quadrupole polarities appropriately[22,23]. These oscillations are more complicated than simple harmonic motion, but they are stable at all amplitudes. A proper array of quadrupoles doesn't have a dynamic aperture.

The vector potential for a sextupole is

$$A_z = \frac{\mu_0 I_3}{6a^3}(x^3 - 3xy^2) \ . \tag{28}$$

The transverse dimensions are coupled together, and keeping the generality of two transverse dimensions introduces too many complications, so assume $y, p_y = 0$. Then

$$H_T = \frac{c^2}{H_0}\left\{\frac{p_x^2}{2} - \frac{e\mu_0 I_3}{6a^3}x^3\right\} , \tag{29}$$

and there is no potential well independent of the sign of I_3 (Figure 17). You might think of a clever scheme to have one sextupole polarity when $x > 0$ and the opposite when $x < 0$, but the particle that starts out in this array with the wrong initial phase is lost. The difference from a quadrupole lattice is that the latter is focusing or defocusing independent of initial oscillation phase of a particle. Combining a quadrupole and sextupole (Figure 17)

$$H_T = \frac{c^2}{H_0}\left\{\frac{p_x^2}{2} - \frac{e\mu_0 I_2}{4a^2}x^2 - \frac{e\mu_0 I_3}{6a^3}x^3\right\} , \tag{30}$$

and for $eI_2 < 0$ there is a potential well at small oscillation amplitude, small H_T, and the motion is approximately simple harmonic. As H_T increases the cubic term in the potential becomes important, and for

$$H_T > H_T(\max) = \left|\frac{e\mu_0 I_2^2}{12 I_3^3}\right| \tag{31}$$

the motion is unbounded. The maximum value of displacement is $x = -aI_2/I_3$; the sign of I_3 determines whether particles escape in the +x or -x direction but not whether the motion is stable. The sextupole field has introduced a maximum stable amplitude, a dynamic aperture.

The model above is a great simplification of an accelerator where there are dipoles, quadrupoles of alternating polarity, and non-linear fields of different strengths. As far as a particle is concerned these magnetic elements are periodic because they are encountered each revolution. This introduces another important parameter, the phase advance of the oscillation between non-linearities. There is a second simple model that illustrates the importance of the phase advance. It is a ring

* For the SSC at the injection energy of 2 TeV: $p_z = 2$ TeV/c, $|p_x|, |p_y| = 5$ MeV/c, $|eA_z| = 0.5$ MeV/c, and 500 eV/c for the quadrupoles and persistent current sextupoles, respectively.

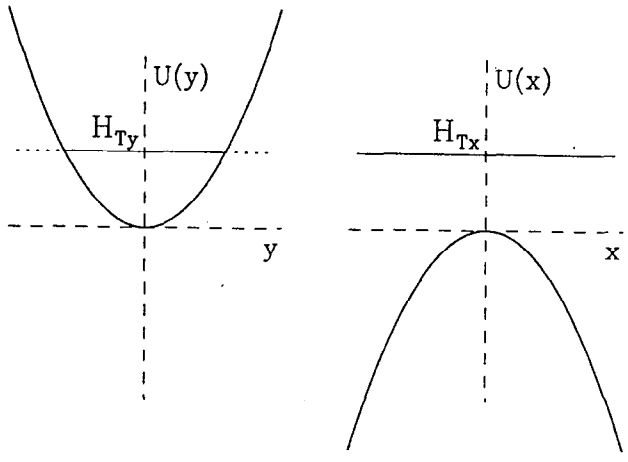

Figure 16: Potential energy curves for vertical and horizontal motion when $eI_2 > 0$.

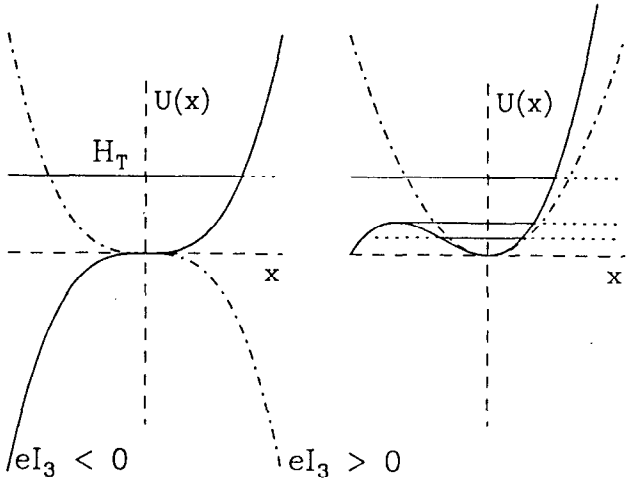

Figure 17: Potential energy curves for a sextupole (left hand side) and combined quadrupole and sextupole (right hand side).

composed of quadrupoles and dipoles and a single discrete sextupole where the phase of the oscillation due to the quadrupoles advances by $2\pi Q_0$ between passages through the sextupole. This system can be analyzed by constructing a map that takes the position and momentum after N passages around the ring and through the sextupole, and propagates them around the ring and through the sextupole to give the position and momentum on turn N+1[24,25]. The results are shown in Figure 18. The motion can be categorized as:

I) Simple harmonic motion or modest departures from it due to the sextupole non-linearity. The maximum stable amplitude depends on the tune, Q_0. At $Q_0 = 1/3$ there are no stable oscillations as a consequence of having a sextupole non-linearity.

II) Oscillatory motion that does not pass through the origin. These are oscillations about a local potential minimum that is not at the origin.

III) Chaotic motion where sometimes the amplitude of oscillation becomes infinite.

These three types of motion can also be illustrated by a Poincaré map, a scatter plot of $\{x, p_x\}$ on successive turns. The Poincaré map for $Q_0 = 0.211$ is shown in Figure 19. Small amplitude particles near the center of the map move in a regular path (type I motion). As the amplitude increases there is a five-fold island structure associated with the nearby rational fraction $Q_0 = 1/5$, and particles in that region jump from island-to-island on successive turns. Over a long time smooth paths appear in all the islands (type II). Outside of the island structure the motion becomes chaotic and unbounded (type III). The boundary between the regular motion and the chaotic behavior is the dynamic aperture.

In both these models sextupole fields have led to a dynamic aperture. The same physics leads to a dynamic aperture in a synchrotron or storage ring. If the dynamic aperture is larger than the physical aperture or larger than the beam, it is not important. That is the case in many accelerators, but not for large superconducting rings where because of superconductor costs there are strong reasons to reduce the coil radius as far as possible. The lower limit on the radius comes from persistent current multipoles at the injection energy which have strong dependences on the coil radius.

2.6 Obtaining Adequate Dynamic Aperture

Any accelerator project involves trade-offs of diverse considerations - performance, commissioning time, cost, politics, etc. High energy hadron colliders must have an adequate dynamic aperture, but that aperture is expensive and one cann't afford to be conservative on all fronts. Going from the need for *adequate dynamic aperture at minimum cost* to technical specifications requires a great deal of judgement for the following reasons.

I. Time Scales - Phenomena occur on different time scales ranging from a) the fraction of a second needed to damp the steering errors that occur when the beam is injected into the collider ring to b) the storage time that can be tens of hours.

II. Persistent Current Decay - Persistent currents is a misnomer; the persistent currents in accelerator magnets decay in time. Some of the causes are basic[26], but the cable and magnet manufacturing processes are more important. Experience with HERA has shown that persistent current decay rates depend on the superconducting

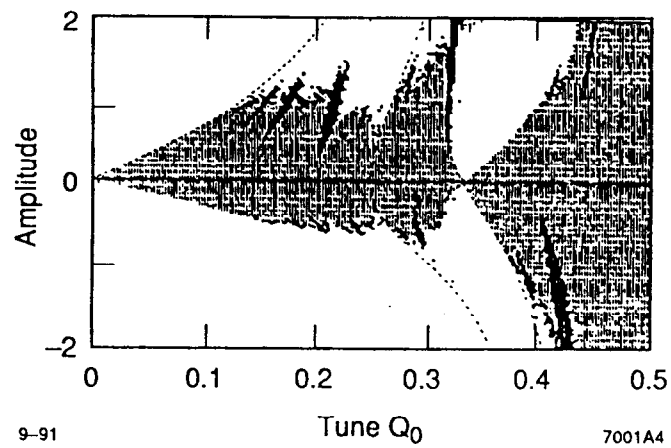

Figure 18: The results of following particles around a ring and through a single sextupole[25]. The shading indicates the type of motion: lightly shaded = I, dark shading = II, blank = III. The "amplitude" has a sign because of different starting phases.

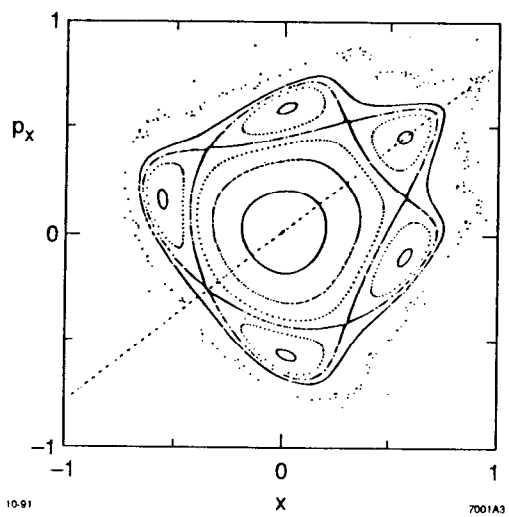

Figure 19: The Poincaré map for $Q_0 = 0.211$[24,25].

cable manufacturer and that the decay rates measured in magnets are usually much longer than those in cable samples[27]. This is not understood completely at the present time.

III. Multipole Corrections - Corrections are possible. The sextupole moment of a test magnet in the dipole electrical circuit can be measured and sextupole correctors adjusted based on that measurement. This is being done at HERA where there are sextupole correction coils wound on the beampipe; two test magnets are needed because of the different properties of the superconducting cable from the two manufacturers. Such a procedure assumes that the sextupole moments have sufficiently small spreads in value and time dependence from magnet to magnet. The uncertainty about the cause of persistent current decay is a complication.

IV. Beam Based Corrections - The beam itself can be used as a diagnostic to understand and improve the dynamic aperture. How much should one rely on this? It does increase the commissioning time.

V. Sensitivity to Assumptions - The specifications are sensitive to assumptions made about the parameters of subsystems and components. Superconductor properties, operating temperature spread, and even the power supply regulation are important.

VI. Non-linear Dynamics - The physics of the dynamic aperture is non-linear dynamics, and that is an active field of research with articles appearing each month in *Physical Review Letters*.

Despite these uncertainties accelerator designers must make choices, and that is where the judgement enters. The discussions in the previous sections are sufficient to understand the considerations that go into the choices. First, the superconducting filament size should be minimized (eq. 19). Research into the properties, metallurgy, and manufacturing of superconducting wires has been successful in increasing the critical current and reducing the filament size. This research was motivated in part by the SSC, and these advances are incorporated into the SSC and LHC designs. Second, the aperture at the injection energy is the most critical because i) the persistent current (relative to the transport current) is largest there, ii) the beam energy is low and the beam is less rigid, and iii) the beam is large - adiabatic damping[22] makes the size proportional to $E^{-1/2}$. Raising the injection energy increases the effective dynamic aperture. Third, the beam size can also be reduced by increasing the number of quadrupole magnets that focus the beam. The cost is an increase in circumference for the same beam energy. Fourth, all of the non-linear multipoles decrease as strong powers of the coil radius (eq 20). For example, the persistent current sextupole varies as a^{-4}, and this sextupole moment can be reduced by a factor of two with less than 25% increase in a. All of these ways of increasing the dynamic aperture were used in the changes of the SSC design made in early 1990. Sextupole correction windings were removed from the design at the same time. They were judged to introduce to many engineering complications.

2.7 Perspective on Superconducting Accelerator Magnets

Superconducting magnets are the most important advance in accelerator technology during the last decade. They have allowed us to reach almost 2 TeV in center-of-mass energy at the Tevatron, are an essential part of HERA where lepton-hadron scattering soon will be explored at qualitatively new energies and momentum transfers, and without them we wouldn't be planning the SSC and LHC. The major milestones during the past ten years include i) the design, construction, and operation of the Tevatron, the first large scale superconducting accelerator, ii) the HERA proton ring which is the first large scale superconducting accelerator produced by industry, and iii) the progress in superconducting wire manufacture summarized by Figure 12. High energy physics has drawn on all these advances in the SSC and LHC designs.

What are the prospects for the future? Much of the progress with NbTi cable came from understanding and improving manufacturing techniques. These techniques no longer limit the critical current, and research is concentrating on intrinsic properties of the conductors such as the flux pinning force. There could be improvements of a factor of two or more in the critical current if this research is successful[19].

The June 1991 issue of *Physics Today* was devoted to high-T_C superconductors, and it has interesting review articles for non-specialists. One of them, "Critical Currents and Magnet Applications of High-T_C Superconductors" by David Larbalestier[28] discusses the issues of interest to high energy physics. The major one is the critical current, J_C, that is closely related to the presence of "weak-links" and flux pinning. High-T_C superconductors have regions of high J_C, but there are weak-links between these regions that make the effective critical current much less than J_C in these good regions. Empirical approaches to conductor fabrication have led to ways to break this weak-link barrier and have shown that weak-links are not intrinsic properties of high-T_C superconductors. Other experimenters have been successful at increasing the flux pinning forces by modifying the conductor fabrication process. Some impressive results have been obtained including a current density of 100 A/mm^2 at 77 K and 1 T, and exceeding 100 A/mm^2 at 4.2 K and 25 T.

High-T_C superconductivity is a rapidly developing field. Quoting from Larbalestier's article: "Those who have been striving to make high-field magnets with high-temperature superconductors have gone through an initial period of great euphoria (1987-88) followed by an interlude of some gloom (1988-89). But 1989 gave us the breakthrough to high transport critical current, and the subsequent developments make us confident that some of the high hopes of the early days will be realized. There is still tremendous scientific interest in high-temperature superconductivity, and the materials problems are slowly being understood and controlled. All this progress within just five years of that innocent-sounding paper of Bednorz and Müller is surely extraordinarily and very promising." High-T_C superconductors could impact high energy physics strongly in the future.

3. SUPERCONDUCTING RF

3.1 Radio Frequency (RF) Cavities

An RF cavity is sketched in Figure 20. RF power with (angular) frequency ω is coupled into the cavity, and it produces electric and magnetic fields $\mathbf{E}(\mathbf{r},t) = \mathbf{E}(\mathbf{r})\exp(i\omega t)$, $\mathbf{H}(\mathbf{r},t) = \mathbf{H}(\mathbf{r})\exp(i\omega t)$. The cavity dimensions and frequency ω are such that a resonant mode with a large component of electric field along the direction of the beam is excited. The effective voltage, V_{EFF}, is the energy gain per unit charge that a beam particle experiences (including any transit time effects) and the gradient, G, is the effective voltage divided by the cavity length.

The cavity is made out of a conductor. Fields inside that conductor near the surface decay exponentially with a characteristic distance given by the skin-depth $\delta = (2/\mu_0\omega\sigma)^{1/2}$ where σ is the conductivity. There are currents flowing in the cavity wall, and there are ohmic losses as a result. The power loss per unit surface area is

$$P_S = \frac{1}{2} R_S H_S^2 \tag{32}$$

where $R_S = 1/\sigma\delta$ is the surface resistance and $H_S = |\mathbf{H}(\mathbf{r})\times\mathbf{n}|$ ($\mathbf{n}$ is a unit vector normal to the surface) is the surface magnetic field. The energy lost per radian of the RF cycle is given by an integral over the surface

$$\Delta E = \frac{R_S}{2\omega} \int_S H_S^2 dA \ , \tag{33}$$

and the electromagnetic field energy by the volume integral

$$W = \mu_0 \int_V |\mathbf{H}|^2 dV \ . \tag{34}$$

The quality factor of the cavity mode,

$$Q_0 = \frac{W}{\Delta E} \ , \tag{35}$$

is a property of the cavity and the mode that is excited; it depends on the cavity geometry and material. It is called the "unloaded Q" because there can be additional losses due to the beam and/or external loads and these are not included in the energy loss given by eq. 33. The "shunt impedance" looks like it comes from Ohm's Law and the expression for resistor power

$$R_A = \frac{(V_{EFF})^2}{P} = Q_0 \frac{(V_{EFF})^2}{\omega W} \ ; \tag{36}$$

$P = \Delta E\omega = \omega W/Q_0$ is the power dissipated in the wall.

The advantage of superconducting RF is a low surface resistance. This means i) a high Q_0, ii) a large stored energy and a large effective voltage for a small amount of

power, and iii) a large shunt impedance. These are crucial for high energy electron storage rings.

3.2 RF Superconductivity in High Energy Storage Rings

An electron of energy E loses an average energy

$$U_0 = C_\gamma \frac{E^4}{\rho} \tag{37}$$

per turn to synchrotron radiation[29]. In this equation ρ is the bending radius and $C_\gamma = (4\pi/3)r_e/(mc^2)^3 = 8.85\times10^{-5}$ m-Gev^{-3}. The RF must have sufficient voltage to make up this energy loss (plus some extra to retain particles with energy losses that fluctuate above the average), and, if the beam current is I, it must transfer power $(I/e)U_0$ to the beam to make up for the synchrotron radiation power. There is some additional "beam loading" of the RF, power that must be supplied to the beam by the RF system, that is proportional to I^2 and is more important for heavy quark factories. It is discussed later in Section 3.5.

If the RF system has a fixed shunt impedance, the RF power to generate the needed voltage scales approximately as $P \sim V_{EFF}^2 \sim U_0^2 \sim E^8/\rho^2$! This limits the size and energy of electron storage rings, and shows clearly the reason for linear colliders at high energies.

LEP is about as large as an electron storage ring can be, and it is worth looking at the parameters of LEP I operating at 55 GeV given in Table I[30]. The total beam current is 6 mA (3 mA in each of the beams), the energy loss per turn is U_0 = 260 MeV/turn, and the synchrotron radiation power is 1.56 MW. When the other sources of beam loading are accounted for, the total beam loading is about 10% higher. An RF peak voltage of V_{EFF} = 360 MV is required for a 24 hr beam lifetime. LEP I has 128 room temperature, copper RF cavities. Each cavity has five cells along the beam and a large, spherical energy storage cavity at the top. One five-cell cavity is shown in Figure 21. The cavities are driven by klystrons with frequencies that differ by the beat frequency between the accelerating and energy storage cavities. The phase of the beat is adjusted so that the accelerating cavity fields are a maximum when the beams pass through the cavity and the field energy is stored in a high Q mode in the storage cavity in between. This increases the shunt impedance by approximately 1.5.

The beam loading is 13% of the total RF power in LEP I; the other 87%, 12 MW, is used to establish the voltage. It heats the cavity walls. Raising the energy from 55 GeV to 95 GeV without changing the RF system would require roughly $(95/55)^8 \simeq 80$ times the RF power to generate the needed voltage. That's 950 MW, and that's impossible! More cavities could be added, and that would lower the RF power because the product $R_A P$ is the quantity that must be increased by eighty (eq. 36). However, there isn't enough space to fit in the needed cavities without a substantial gradient increase. The maximum gradient of 1.47 MV/m is typical for a room temperature, storage ring RF system that must be on whenever there is stored beam. Significantly higher gradients aren't possible because of the engineering problem of dissipating the heat generated in the cavity walls. (Room temperature

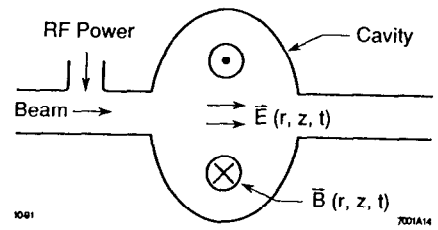

Figure 20: Sketch of an RF cavity.

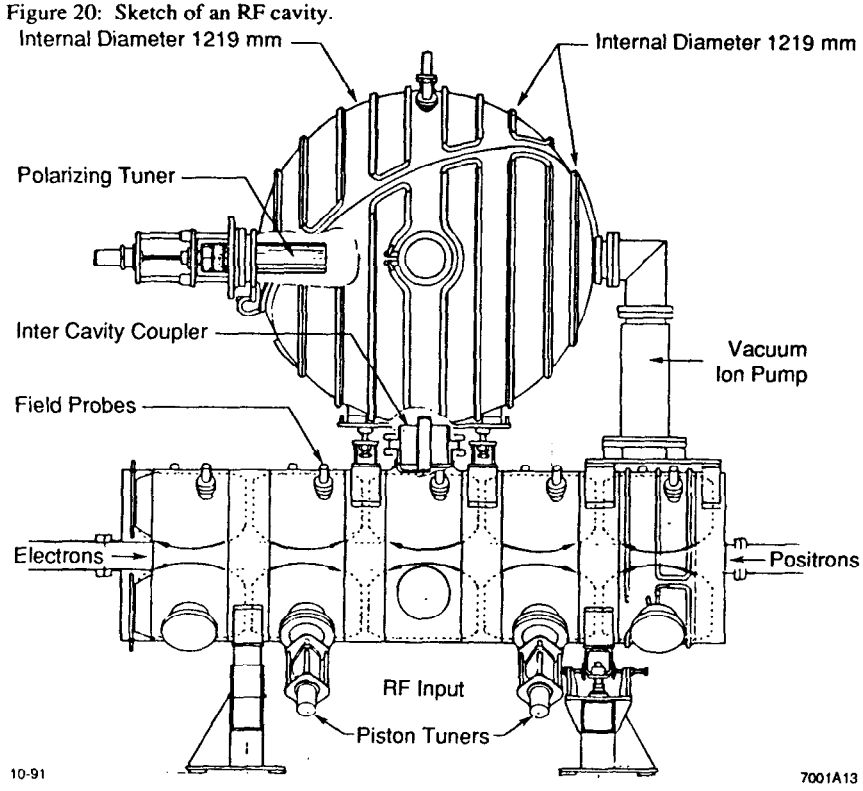

Figure 21: One five-cell cavity of the LEP I RF system[30].

Table I: LEP Parameters

Parameter	LEP I[30]	LEP at 95 GeV[3,31]
RF System	Copper	Superconducting
Circumference	26659. m	
Bending Radius (ρ)	3096. m	
Nominal Current per Beam	3.0 mA	
Beam Energy (E)	55. GeV	95. GeV
Synchrotron Radiation Loss (U_0)	260. MeV/turn	2.31 GeV/turn
Synchrotron Radiation Power	1.56 MW	13.9 MW
Total Beam Loading	1.75 MW*	--
Peak RF Voltage (V_{EFF})	360. MV	2.7 GV
Number of RF Cavities	128	256
Shunt Impedance per cavity	85. MΩ/5-cell	1.4×10^{12} Ω/4-cell
Active Cavity Length	2.13 m/5-cell	1.70 m/4-cell
Maximum gradient (G)	1.47 MV/m	6.1 MV/m
Power of generate V_{EFF} (eq. AA)	12. MW	20. kW

* indicates a parameter calculated from those given in the reference.
-- Insufficient information to estimate.

linear accelerators have much higher gradients. They run with a low duty cycle to solve the heating problem.)

An RF system with a higher shunt impedance and a higher gradient is needed for LEP to operate above the W^+W^- threshold. That is the role of superconducting RF. Table I shows the remarkable difference in the parameters of LEP with superconducting RF; this column of the table is discussed in detail in Section 3.4.

3.3 Q_0 and Gradient Limits

The performance limits of a superconducting RF system come from a combination of fundamental and practical factors. Begin by considering the fundamental limits.

In the BCS theory of superconductivity the Cooper pairs have an energy associated with pairing equal to $2\Delta(T)$. The pairing energy at T = 0 K is proportional to the critical temperature, and $2\Delta(0) \approx 3.5kT_C$ (k is Boltzmann's constant), and when $T < T_C/2$, $\Delta(T) \approx \Delta(0)$[7]. Thermal processes can break pairs apart giving some normal electrons. The density of these normal electrons, n_E, and the Cooper pair density, n_0, are related as[32]

$$n_E = 2n_0 \exp(-1.75T_C/T) \qquad (T < T_C/2) \quad . \tag{38}$$

The electromagnetic fields penetrate into the superconductor by an amount given by the London penetration depth, λ. These fields interact with the normal electrons. This leads to losses that depend on the density of normal electrons and the time derivative of the field

$$P_S \sim n_E(T)\,(\omega H_S)^2 \quad . \tag{39}$$

Combining eqs. 32, 38, and 39 gives the result of the two fluid model that is a good approximation to the BCS surface resistance[32]

$$R_S = A\,\frac{\omega^2}{T}\,\exp(-1.75T_C/T) \quad . \tag{40}$$

The constant A depends on the material through the London penetration depth, the correlation length, electron mean-free-path, etc. In addition, there are losses and a residual resistivity, R_R, due to surface properties that not associated with superconductivity such as residual films from cleaning and oxide layers. The total surface resistance is

$$R_S = A\,\frac{\omega^2}{T}\,\exp(-1.75T_C/T) + R_R \quad . \tag{41}$$

Figure 22 compares the temperature and frequency dependences of the surface resistance with eq. 41 and with the complete BCS theory[32].

At 500 MHz Nb at 4.2 K has R_S = 70 nΩ as compared to R_S = 5.8 mΩ for copper[32]. A superconducting Nb and a room temperature Cu cavity of the same geometry have Q_0's in the ratio $Q_0(Nb)/Q_0(Cu) \sim 8\times10^4$. The Nb cavity requires 1.2×10^{-5} of the RF power of the Cu cavity! Of course, the power is dissipated at 4.2 K, and that requires about 500 times the AC mains power for a refrigerator when the technical efficiency and the Carnot efficiency, $\eta_{CARNOT} = T_{COLD}/(T_{HOT}-T_{COLD}) \approx 0.014$, are taken into account. There is still a factor of almost 200 lower energy consumption with a superconducting RF system.

The fundamental limit to the gradient comes from breakdown of superconductivity when the surface field exceeds a critical field value, B_{MAX}. The critical field depends on the thermodynamic critical field, B_C, and $\kappa = \lambda/\xi$ (Section 2.1)[33]

$$B_{MAX} = \begin{cases} 0.75\,B_C & ,\ \kappa \gg 1 \text{ (type II)} \\ 1.2\,B_C & ,\ \kappa = 1 \\ B_C/\sqrt{\kappa} & ,\ \kappa \ll 1 \text{ (type I)} \quad . \end{cases} \tag{42}$$

The calculation leading to this result takes into account i) a superheated state that can exist because of the entropy change associated with the first order phase transition from a superconducting to a normal state and ii) the nucleation time for flux lines that is much longer than a typical RF period[32]. The maximum surface field for Nb, the most common cavity material, is $B_{MAX}(T = 0) = 240$ mT. This corresponds to an accelerating gradient G = 50 MV/m for a typical cavity geometry. This is the fundamental accelerating gradient limit of Nb cavities.

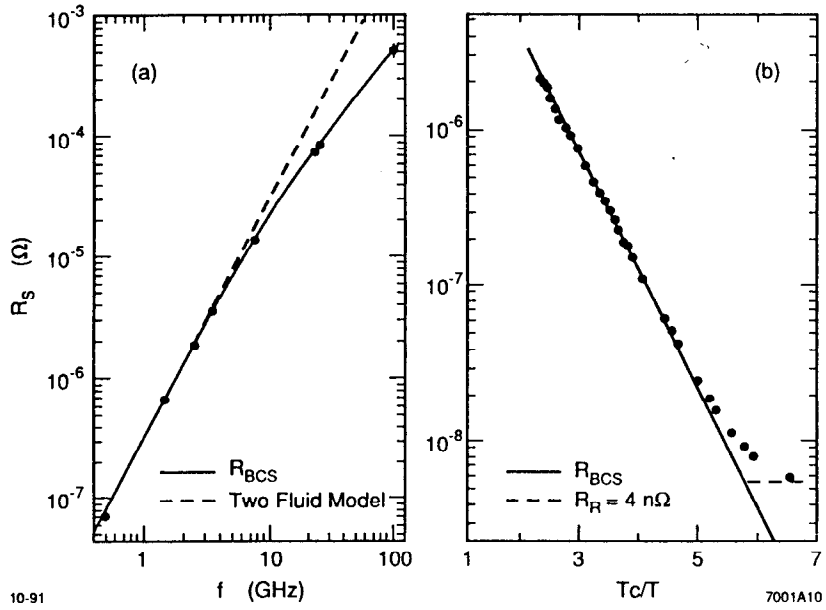

Figure 22: Comparison of the frequency dependence (a) and temperature dependence (b) of the surface resistance of Nb with BCS theory[32]. Eq. (41) is the surface resistance in the two fluid model.

Niobium cavities reach surface fields of 20 to 60 mT, and cavities produced in industry have maximum gradients in the 5 to 10 MV/m range. Clearly, the maximum gradient is determined by factors other than the fundamental limit. These factors are technological in nature, and solving them has been the reason for progress in superconducting RF that is summarized in Figure 23. Problems identified and cured include the following.

I. Multipacting or resonant electron emission. In the simplest form of this process an electron emitted from the surface is accelerated away from the cavity wall during part of the RF cycle and then is accelerated back towards the wall (when the RF phase changes sign) striking near the spot where it was emitted. If more than one secondary electron is emitted on impact, a resonant build-up of current occurs, and the cavity breaks down when this current gets too high. All high gradient RF cavities multipact. Repeated application of high power RF or coating can modify the surface and reduce the secondary emission coefficient of room temperature cavities, but neither of those techniques is appropriate for superconducting cavities.

The multipacting phenomena can be more complicated than described above; several RF cycles can pass between emission and striking the wall again, and the emission and impact points can be different. It was discovered by serendipity that cavities with a spherical shape such as shown in Figure 24 do not multipact[34]. Calculations showed that electrons drift towards the equator of the cavity where there is no accelerating component of the electric field[35]. Many superconducting cavities have been made with spherical and elliptical shapes, and they do not multipact.

II. Defects. Fabrication introduces a variety of defects including chemical residue, weld splatter, and weld holes. These defects heat-up and can be found by temperature mapping. Diligent work locating and understanding the causes of defects has lead to improvements of fabrication techniques and a substantial reduction in the number of defects.

III. Increasing the Thermal Conductivity. If a defect gets hot enough it causes a quench. The temperature a defect reaches comes from the balance of heating which is proportional to G^2 and cooling due to heat conduction through the surrounding Nb. Increasing the thermal conductivity increases the maximum gradient. This has been done in collaboration with Nb manufacturers, and the result is a marked improvement in gradient.

The present gradient limit is due to field emission which is quantum mechanical tunneling of electrons out of the surface. The field emission current loads the cavity and results in a Q reduction at high gradients. The work function of Nb, 4 eV, is too high to account for the field emission, and the present thinking is that field emission is coming from defects, impurities, chemical residues, etc. Studies of DC field emission has shown that heat treating Nb up to 1100°C to 1400°C cleans the surface and reduces field emission substantially[36]. This is shown in Figure 25 that compares chemically and heat treated cavities and shows the current state-of-the-art.

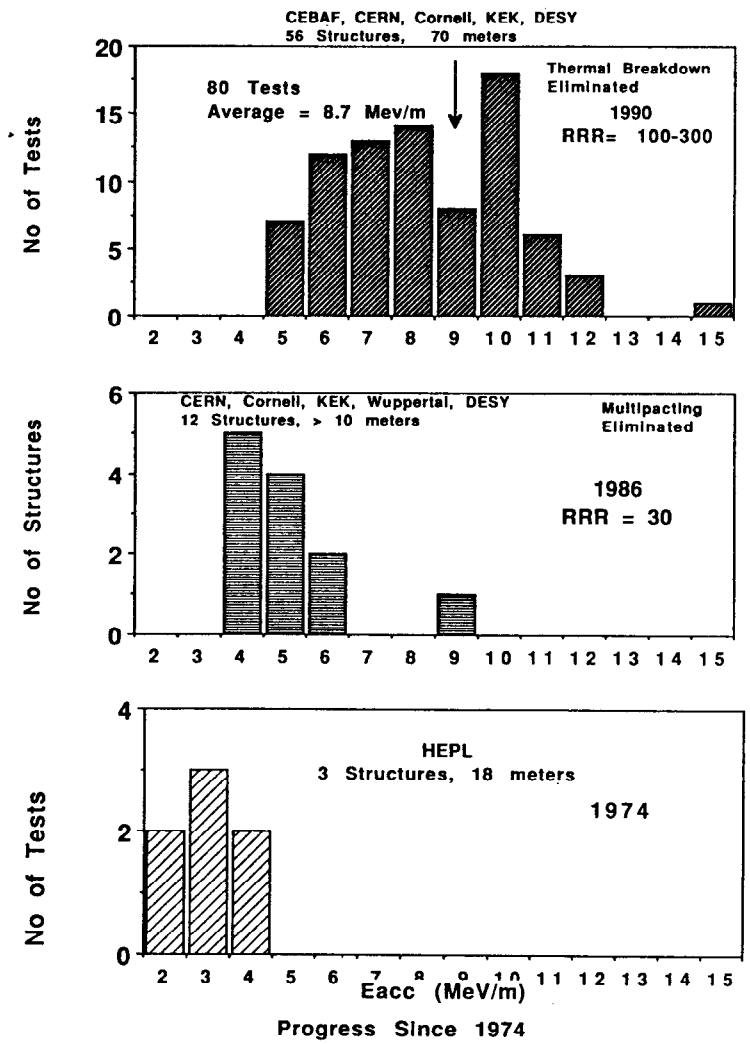

Figure 23: Superconducting cavity gradient improvements[38]. Multipacting was eliminated between 1974 and 1986, and the thermal conductivity was increased between 1986 and 1990.

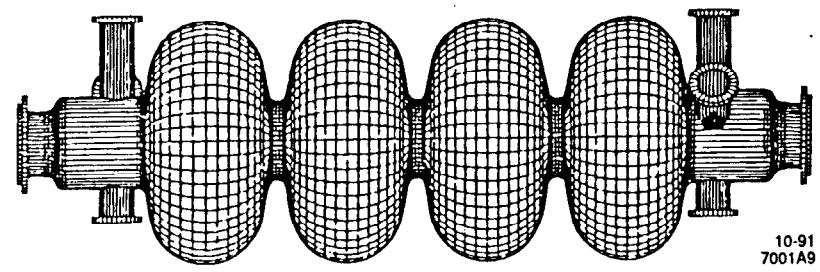

Figure 24: The 4-cell cavity module foreseen for LEP II[32,39]. Most of the waveguides at the ends are for loading higher modes (Section 3.5).

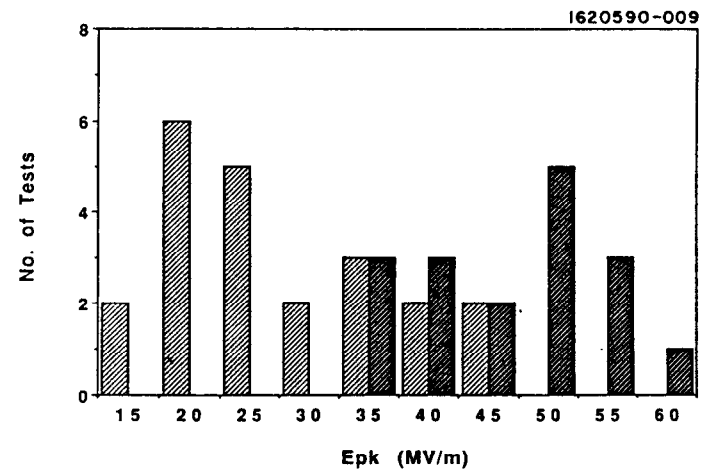

Figure 25: A comparison between the maximum surface fields achieved by the same cavities with (dark cross hatch) and without (light cross hatch) heat treatment at T = 1100°C - 1400°C[36]. The gradient is roughly one-half the surface field.

3.4 LEP above the W-Pair Threshold and as a Z-Factory

As Table I shows, the energy loss per turn and peak RF voltage increase by roughly an order of magnitude when the LEP energy is raised from 55 GeV to 95 GeV. Superconducting RF will make it possible to run above the W-pair threshold! It does this by increasing the accelerating gradient and changing the RF power economics.

The total cavity length is being increased from 273 m to 435 m by filling all available straight sections, and a gradient of 6.1 MV/m is being planned. This can be expected for commercially manufactured cavities. Some of the cavities have been made by forming sheet Nb and some are likely to be made from a copper shell with about 1 μm of Nb sputtered on the inside. That is all the Nb needed,[37] and it is less expensive because of the high cost of niobium.

The shunt impedance per cell is increased by about four orders of magnitude, and, as a result, 20 kW of RF power produces the needed V_{EFF} vs 12 MW needed to generate one-tenth the voltage with the room temperature, copper RF system. The RF power can now be used to make up synchrotron radiation power instead of generating voltage.

The change from room temperature to superconducting RF will increase the LEP luminosity at the Z also. Once it is installed, there is spare RF power when LEP is running at the Z unless the beam current is raised. The luminosity of an electron-positron storage ring collider is proportional to the total beam current, and the spare RF power will be used to raise the total current and the luminosity. Because of the beam-beam interaction in storage ring colliders, the total current must be raised by increasing the number of bunches rather than the current per bunch. Doing this, the luminosity at the Z should increase by over an order of magnitude to above $10^{32}cm^{-2}s^{-1}$.

3.5 Wake Fields

So far the discussion has concentrated on the accelerating mode. An RF cavity has many resonant modes, just like a pillbox cavity. The accelerating mode is almost always the lowest frequency, or fundamental, mode, and the other modes are usually called higher modes. These higher modes affect the beam also. Power is not put into them by a power source; they are excited by the beam. Figure 26 shows the results of a calculation of a beam passing through a LEP cavity cell[40]. Initially there are no fields in the cavity. (Why are there no fields in the fundamental mode? The figure shows only part of the picture. By superposition the fields in the fundamental produced by a power source can be added to give the total field.) As the beam enters fields begin to fill the cavity, and, after it has exited, fields remain in the cavity.

These beam generated fields are called "wake fields". There are longitudinal and transverse wake fields. The longitudinal wake field is an electric field in the direction the beam travels; it accelerates or decelerates. The transverse wake fields are perpendicular to the direction of travel, and they deflect the beam. Figure 27 shows the longitudinal "wake potential" - the longitudinal wake field a particle experiences integrated over the structure. Figure 27a shows that the wake potential is negative on the short-time scale as it must be because energy is transferred from the beam to the

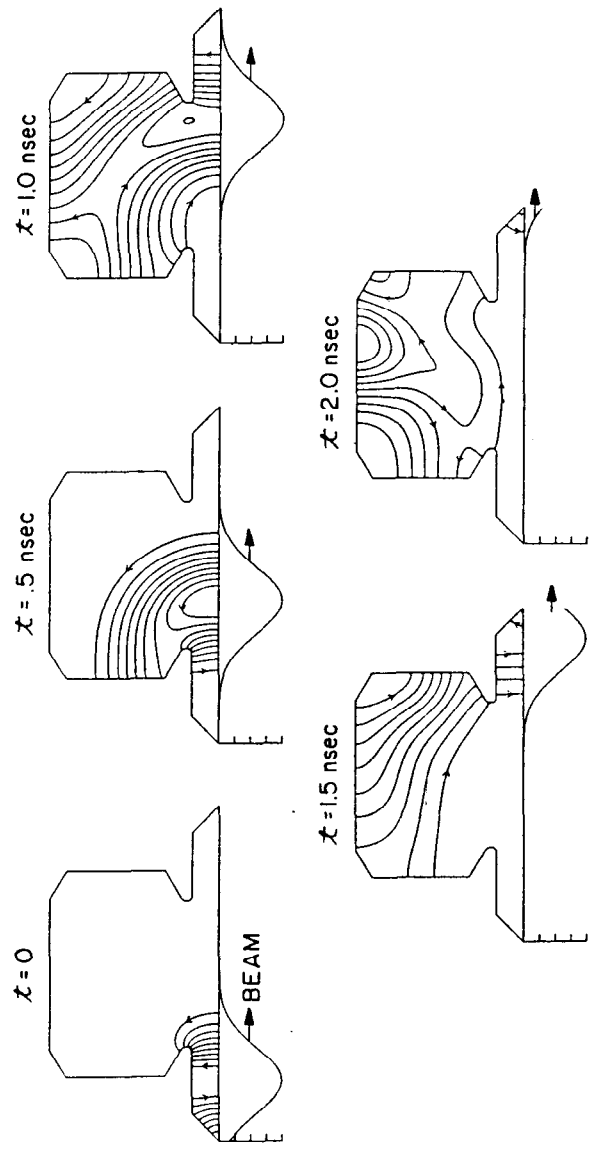

1360989-082

Figure 26: Field lines of total current density as a Gaussian bunch passes through a LEP RF cavity cell[40].

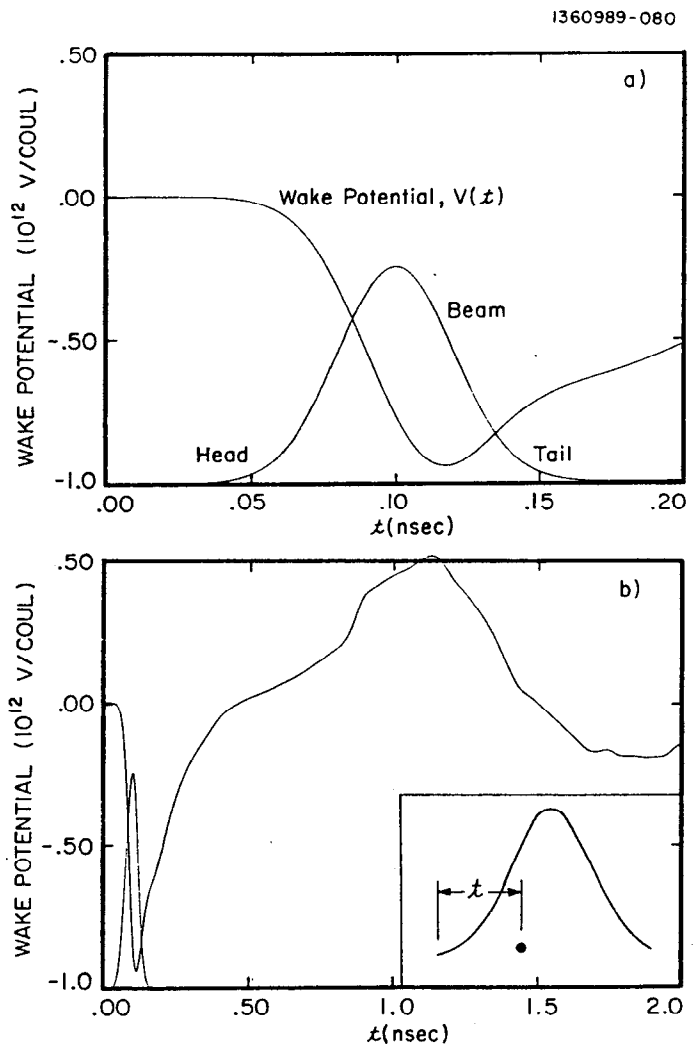

Figure 27: The wake potentials for a 6 mm long, 1 C bunch traveling through a CESR cavity shown on two different time scales. The inset defines the time t.

cavity fields. The cavity fields can be described by a linear superposition of fields in the resonant modes, and on a longer time scale the ringing of the dominant modes is seen (Figure 27b).

Wake fields are bad, they cause:

I. Beam Loading. The wake potential is proportional to the single bunch current, $V_W \propto I_S$. The energy loss or beam loading from wake fields,

$$\Delta E = \int V_W(t) I_S(t) dt \ , \tag{43}$$

is proportional to I_S^2. This was mentioned in Section 3.1. It increases the RF power needed and can cause heating of beamline components.

II. Single Bunch Instabilities. The head and tail of a bunch experience different forces because of the variation of wake fields over the length of the bunch. This is the cause of longitudinal single bunch instabilities. The transverse wakefields vary over the length of the bunch also. They deflect the head and tail differently and lead to transverse single bunch instabilities.

III. Coupled Bunch Instabilities. Fields generated by a bunch decay with time constants proportional to the Q's of the resonant modes excited. For sufficiently high Q's fields last until the next bunch enters the cavity. This gives the bunches a way to accelerate and deflect each other and can lead to multiple bunch or coupled bunch instabilities.

Roughly speaking, there are two ways to affect wake fields. First, the geometry of the cavity near the beam affects the short-time wake fields that cause beam loading and single bunch instabilities. In general, wake fields are reduced by making the beampipe larger and by making gradual geometry changes near the beampipe. These also reduce R_A/Q_0, the ratio of the fundamental mode shunt impedance and its unloaded Q, and may not be possible when RF power consumption is a primary concern. It isn't a coincidence that the wakefields and R_A/Q_0 are affected by the geometry near the beam pipe; both are measures of the coupling between beam and cavity fields. The second way to affect wake fields is with the Q's of resonant modes. The Q's do not influence the short-time wakefield, but the decay time constant is proportional to Q and the higher the Q's, the higher the potential for coupled bunch instabilities.

The use of superconducting RF affects the wake fields in both ways. The short-time wake field tends to be lower than with a room temperature RF cavity because i) the geometry changes near the beampipe are gradual - that's a feature of the spherical shape needed to eliminate multipacting, and ii) with a high Q_0 the beampipe can be large while still having adequate shunt impedance. The other resonant modes have high Q_0's also, and there would be severe coupled bunch instabilities if the Q's were not reduced. This is done by "loading" these modes. Waveguides with coupling ports or antennae at the cavity are used. The higher mode fields couple to the waveguides and are absorbed in room temperature loads at the other end. Most of the waveguides at the ends of the LEP 4-cell cavity shown in Figure 24 are for loading the higher modes. They are not installed in the cells themselves because that would cause

multipacting around the waveguide openings. With such loading the Q's of higher modes can be reduced to $Q \sim 10^4$ from $Q_0 \sim 10^9$. This is adequate for a large ring like LEP with bunches that are far apart.

3.6 Superconducting RF for B-Factories

The earlier sections have concentrated on the use of superconducting RF to increase the energy of electron storage rings. It is being discussed widely for B-factories also. It is part of the Cornell[41], DESY[42],and INP (Novosibirsk)[43] baseline designs and an upgrade option for CERN[44] and KEK[45]. The parameters of the CERN B-factory in Table II are representative. The beam loading is 80% and 73% in the low energy and high energy rings, respectively. Generating voltage is not the dominant RF power consumer, and the reason for considering superconducting RF is related to wake fields.

The total wake field that can be represented schematically as

Total Wake field = (Number of RF cells)×(Wake field/cell)
+ Wake fields from other components

The wake fields from other components can be reduced with careful design. The superconducting RF strategy addresses the first term. It is to reduce the number of RF cells by using the higher gradient possible with superconducting RF. There is a lower limit to the number of cells set by other considerations such as the amount of power that can propagate through an RF window. The wake field per cell is reduced by increasing the beampipe radius also. This lowers the shunt impedance somewhat, but that's not a dominant consideration with such heavy beam loading.

B-factories have a large number of bunches; that's the only way to get high luminosity with the constraints imposed by the beam-beam interaction. The bunches are close together, 12 m or 40 ns in the CERN design, and higher mode Q's must be reduced to $\sim 10^2$ to prevent severe coupled bunch instabilities. This is accomplished in two ways. First, single cell cavities are used. Multicell cavities have coupled modes with different field strengths in different cells. Some of these modes are "trapped modes", modes that have low fields in the end cells. It is impossible to couple strongly to trapped modes with higher-mode loading waveguides on the beampipe, and the waveguides must be on the beampipe because of multipacting. Single cell cavities avoid trapped modes. Single cell cavities would probably be used even without this consideration. The RF window power limit favors single cells also.

Second, with a large radius beampipe higher modes propagate in the beampipe, and it serves double duty as beampipe and higher mode waveguide. Lossy material placed on a room temperature portion of the beampipe is the RF load. Figure 28 shows the Cornell superconducting cavity. On one end the beampipe is circular, and on the other it is fluted so that the lowest frequency deflecting mode propagates to the absorber. With this type of cavity $Q \sim 100$ can be achieved.

Why aren't all B-factories using superconducting RF? The designs are based on different facilities, and the energy loss per turn and peak voltage are inversely proportional to the bending radius. Larger circumference colliders need less voltage

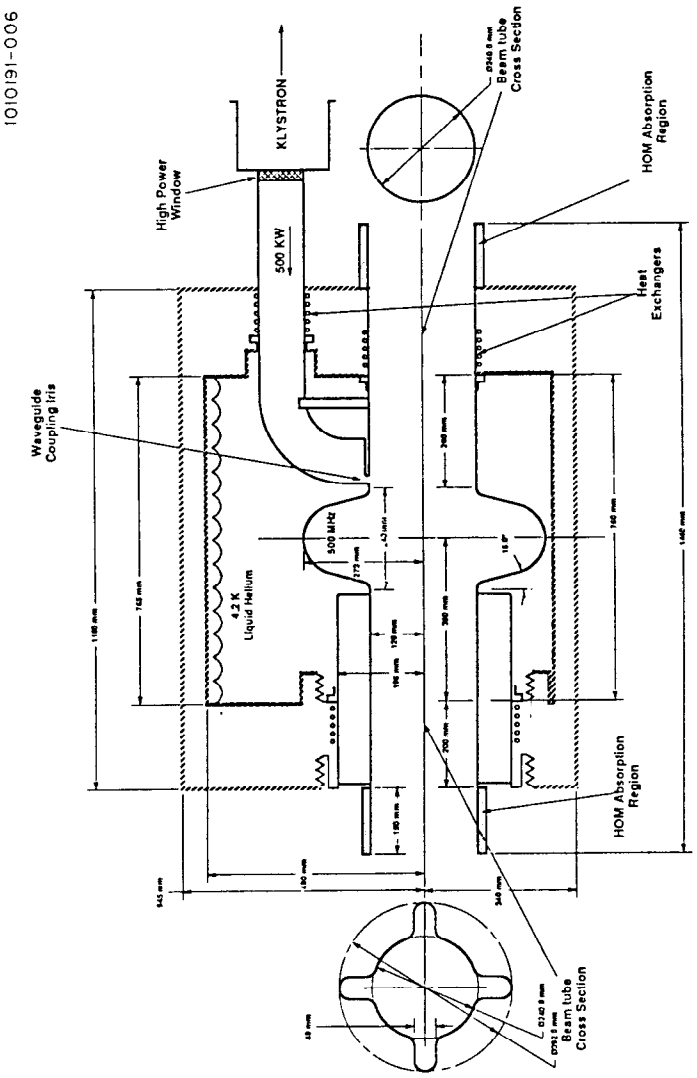

Figure 28: The superconducting RF cavity proposed for CESR-B[41].

Table II: CERN Asymmetric B-Factory[44]

Parameter	Low Energy Ring	High Energy Ring
Circumference	963.4 m	
Bending Radius	65.0 m	
Luminosity	10^{33} cm^{-2}s^{-1}	
Current per Beam	1.28 A	0.56 A
Number of Bunches	80	
Current per Bunch	16 mA	7 mA
Beam Energy	3.5 GeV	8.0 GeV
Synchrotron Radiation Loss	0.3 MeV/turn	5.6 MeV/turn
Synchrotron Radiation Power	0.39 MW	3.1 MW
Total Beam Loading	0.56 MW	3.2 MW
Peak RF Voltage	2.0 MV	13. MV
RF System	Copper	
Number of RF Cavities (single cell)	4	20
Accelerating gradient	1.6 MV/m	2.2 MV/m
Total RF Power	0.70 MW	4.4 MW

and fewer cavities. In addition, superconducting cavities in a B-factory would be running with heavy beam loading and extremely strong higher mode damping. This is outside our present experience and makes superconducting RF more speculative and a less attractive option for large circumference B-factories.

3.7 Linear Colliders

The luminosity of a collider is given by

$$\pounds = \frac{1}{4\pi} \frac{N^2 f_C}{\sigma_H \sigma_V} H_D \tag{44}$$

where N is the number of particles per bunch (assumed to be the same for both beams), σ_H and σ_V are the rms horizontal and vertical sizes, f_C is the collision frequency, and H_D is a luminosity enhancement factor caused by the beams self focusing during the collision. Designing a linear collider involves many considerations and a complex trade-off among them. Figure 29 is R. Palmer's "simplified diagram of the interdependence of collider parameters"[46].

One of the major junctions in that diagram is beamstrahlung which refers to photon radiation in the strong electromagnetic fields at the collision point. Beamstrahlung is characterized by two parameters T and δ[47]. The first of these, T, measures whether the photons have a classical synchrotron radiation spectrum with a critical energy much less than the beam energy ($T \ll 1$) or have energies extending all the way up to the beam energy ($T \geq 1$). Colliders are being designed to be in the classical regime, $T < 1$, to suppress coherent pair production[48]. The second parameter, δ, is defined as ratio of the average radiated energy to the beam energy. It is a rough measure of the center-of-mass energy spread, and usually $\delta \sim 0.1 - 0.3$ is desired. When $T < 1$, the luminosity in terms of δ is[47]

$$\pounds \propto \frac{P_B}{\sigma_V} \left\{ \frac{\delta \sigma_L}{E^3} \right\}^{1/2} \tag{45}$$

where σ_L is the bunch length and P_B is the beam power, the total power of the two beams, given by

$$P_B = 2NEf_C \ . \tag{46}$$

Equation 45 gives one of the central facts about linear colliders - the luminosity is proportional to the ratio of beam power and spot size.

The beam power must come from the AC mains by a series of steps indicated schematically in Figure 30. There is some conversion efficiency, η, $P_B = \eta P_{AC}$, and $\pounds \propto \eta P_{AC}/\sigma_V$. High efficiency and small spots are needed for a reasonable operating cost. One of the factors in the efficiency is η_B, the efficiency with which the beam extracts energy from the RF fields in the accelerator. The transverse dimensions of a linear accelerator scale with λ, the wavelength of the accelerating mode. The field energy per unit length of the accelerator is proportional to the volume times the square of a typical field, $\propto \lambda^2 G^2$. The energy extracted by the beam is NeG, so

$$\eta_B \propto \frac{NG}{G^2 \lambda^2} = \frac{N}{G\lambda^2} \ . \tag{47}$$

Short wavelengths are favored for high efficiency.

Since the typical transverse dimensions of an accelerator scale as λ, a short wavelength implies a small beam hole and large wake fields. The deflecting wake fields are of particular concern; they distort the bunch shape increasing σ_V and creating backgrounds[49]. When the geometry of an accelerator is held fixed, σ_L/λ held constant, and λ varied, the deflecting wake field at the tail of the bunch is proportional to λ^{-3}[47]. This favors long wavelengths, and compromise between efficiency and wake fields is needed.

'Equation 47 implies that η_B can be increased by increasing N, the number of particles per bunch, but the equation is valid only when $\eta_B \ll 1$. The short-time longitudinal wake field produces an unacceptably large energy spread when this inequality isn't satisfied. However, the efficiency can be increased by accelerating multiple bunches spaced in time during the same RF pulse. In that case the RF power source must provide the energy to i) initially fill the accelerator structure with field, ii) accelerate the beam, and iii) make-up the wall losses between bunches. This makes sense as long as the bunches can be spaced close enough that the wall losses between bunches are sufficiently small; then the energy to fill the accelerator structure is shared by many bunches. Almost all linear collider designers are planning on multiple bunches per RF pulse for increasing efficiency.

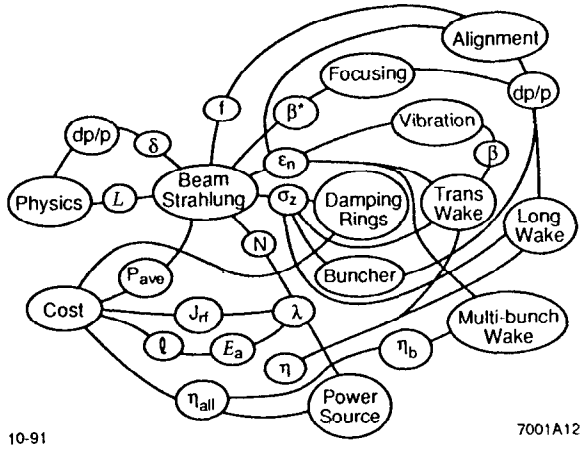

Figure 29: R. Palmer's "simplified diagram of the interdependence of collider parameters"[46].

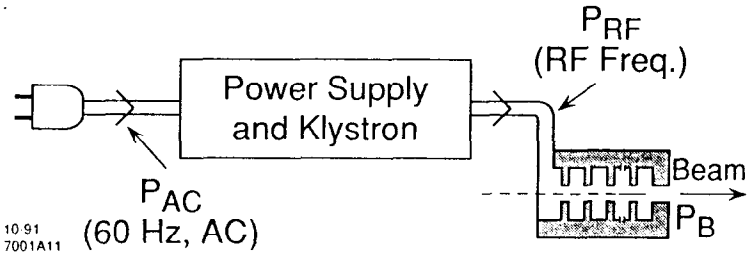

Figure 30: A sketch of the conversion of AC power to beam power.

Multiple bunches are a strong advantage of a linear collider based on superconducting RF. Ideally the RF in such a collider could be on continuously. The energy extraction efficiency, η_B, could be small. All the RF power source has to do is replace the energy extracted by a beam bunch between bunches because the wall losses are small. There is no need to go to short wavelengths as favored by eq. 47, and wake fields become less of a concern. The design of a linear collider based on superconducting RF is being pursued by the TESLA collaboration that has about twenty universities and laboratories in Europe, Japan, and the United States. The idealization above is a simplification, but it has the essence of the argument for using superconducting RF for linear colliders. The next section is more detailed and less simplified.

Figure 31 shows the high energy linear collider options being studied seriously. The ones using room temperature RF have wavelengths ranging from 10 cm to 1 cm. Roughly speaking, the longer wavelength designs have less severe wake field problems, higher construction and operating costs, and are best suited for lower center-of-mass energies. The superconducting linear collider is a very different approach.

3.8 TESLA-TeV Energy Superconducting Linear Accelerator

The present concept of a linear collider based on superconducting RF comes from R. Sundelin[50]. It is now under active study at a number of laboratories and universities that are working together as the TESLA collaboration. This section is based on their 1990 workshop[51]. The workshop proceedings have parameters for ten colliders - center-of-mass energies of 100 GeV, 300 GeV, 500 GeV, 1 TeV and 1.5 TeV each with λ = 10 cm and λ = 20 cm.

For the initial discussion choose E_{CM} = 500 GeV, λ = 10 cm. The parameters are in Table III. The reader interested in making comparisons with room temperature colliders should see the article by Palmer[46] that has parameters for the same center-of-mass energy. What does this collider look like? The acceleration gradient is G = 25 MV/m, so each linac has an active length of 10 km. There must be space for cryogenics, power feeds, and higher mode damping waveguides. The estimate is that with multicell cavities and careful design each meter of active length needs 1.35 m along the beamline[52]. The collider (two linacs and ~1 km for a final focus) is 28 km long. That is about the length of the major axis of SSC. There are two damping rings, one for e^- and one for e^+. Each has a circumference of 3 km, the same size as TRISTAN. The reason for such large damping rings will become clear below.

Wall losses are not negligible, and the RF is not on continuously. It has a 3.2% duty cycle. With that duty cycle, a fundamental mode $Q_0 = 4\times10^9$, and G = 25 MV/m, 52.1 kW of fundamental mode power is dissipated at T = 2 K. This translates into 38.3 MW of AC mains power for the refrigerator. In addition, there is a static heat leak and higher order mode power (eq. 43) at 2 K, and the total AC mains power for the refrigerator is 68.7 MW.

The RF pulse is 1.6 ms long, and 400 bunches are accelerated during the pulse. The minimum bunch spacing is determined by the needed higher mode damping and estimates of the Q reduction possible with the multicell structures that give a filling

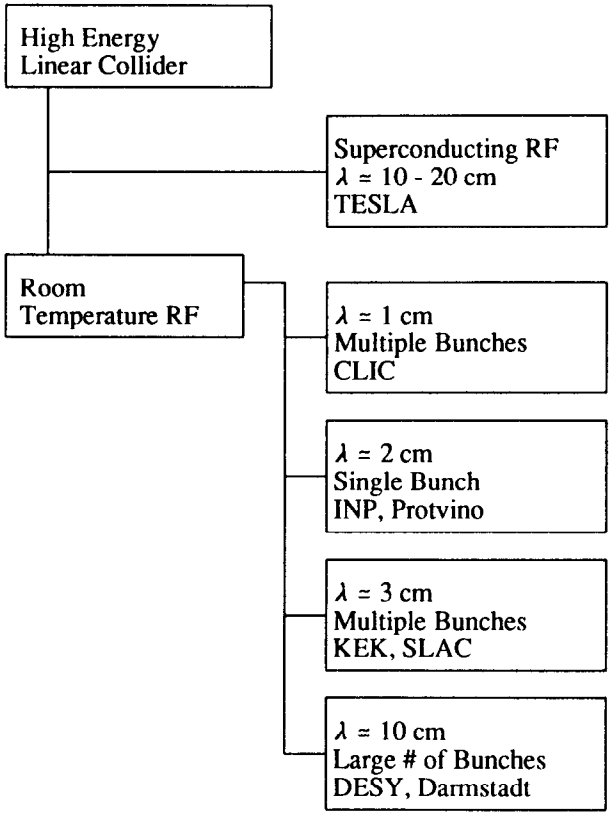

Figure 31: The major directions of linear collider development.

Table III: TESLA at E_{CM} = 500 GeV with λ = 10 cm[53]

Luminosity	$2.1\times10^{33}cm^{-2}s^{-1}$	Gradient	25 MV/m
Total Length	28 km	Damping Ring Circum.	3 km
RF Pulse Frequency	20 Hz	RF Pulse Length	1.6 ms
Beam Bunches/RF Pulse	400	Collision Frequency	8 kHz
Fundamental Mode Q_0	4×10^9	Temperature	2 K
Carnot Efficiency	0.0068	Refrigerator Efficiency	0.2
Fund. Mode Power at 2 K	52.1 kW	Static Heat Leak	20.0 kW
High. Mode Power at 2 K	21.7 kW	Refrig. AC Mains Power	68.7 MW
Peak RF Power	42 kW/m	Particles/bunch	4.2×10^{10}
Bunch Spacing in Linac	4 μs	Beam Power (2 Beams)	26.9 MW
Dumped RF Power	6.9 MW	Klystron Efficiency	0.6
Klystron AC Mains Power	56.3 MW	Overall Efficiency	0.22
RMS Horizontal Size	1.0 μm	RMS Vertical Size	100 nm
£ Enhance from Self Focus	1.9	Beamstrahlung Param (δ)	0.04

factor of 1/1.35. The RF pulse repetition rate is 20 Hz. It takes several hundred μsec to fill the accelerator structure because it has a high Q and the power source has a low peak power. A shorter pulse and higher repetition rate are not optimal because of the long filling time. A large number of beam bunches must be prepared for acceleration during a short time. This is the reason for large damping rings; 400 hundred bunches must be prepared "in parallel".

After the last bunch has passed there are still fields and field energy in the accelerator. That energy must be dumped into external loads at the end of the RF pulse. Adding it to the beam power and assuming a klystron efficiency of 60% gives an AC mains power of 56.3 MW to generate the RF and a total mains power of 125 MW. This would probably increase by 10% - 20% if damping ring, positron production and experimental magnet power were added. The overall efficiency for conversion of AC to beam power is η = (Beam Power)/(AC Power) = 26.9 MW/125 MW = 0.22.

Figures 32 and 33 show the dependences of luminosity, gradient, length, beam power, and AC power on center-of-mass energy[51]. All but the powers are independent of wavelength. Although the surface resistance is higher at shorter wavelengths (eq. 40), the larger cavity volume at longer wavelengths makes the dumped RF and total AC power higher for λ = 20 cm. One can draw conclusions about the two extremes of these plots. Superconducting RF looks like a natural solution for a Z-factory at 100 GeV: i) the collider is smaller than LEP, ii) the power consumption is comparable to today's laboratories, and iii) the gradient is not far above that of presently available, industrially produced cavities. At E_{CM} = 1.5 TeV superconducting RF is pushing on all fronts: i) the collider is over 50 km long, ii) the power consumption is two or more times that of the SSC, and iii) the gradient is close to the fundamental limit for Nb. There needs to be substantial progress improving Q_0's and gradients before superconducting RF is viable at this energy.

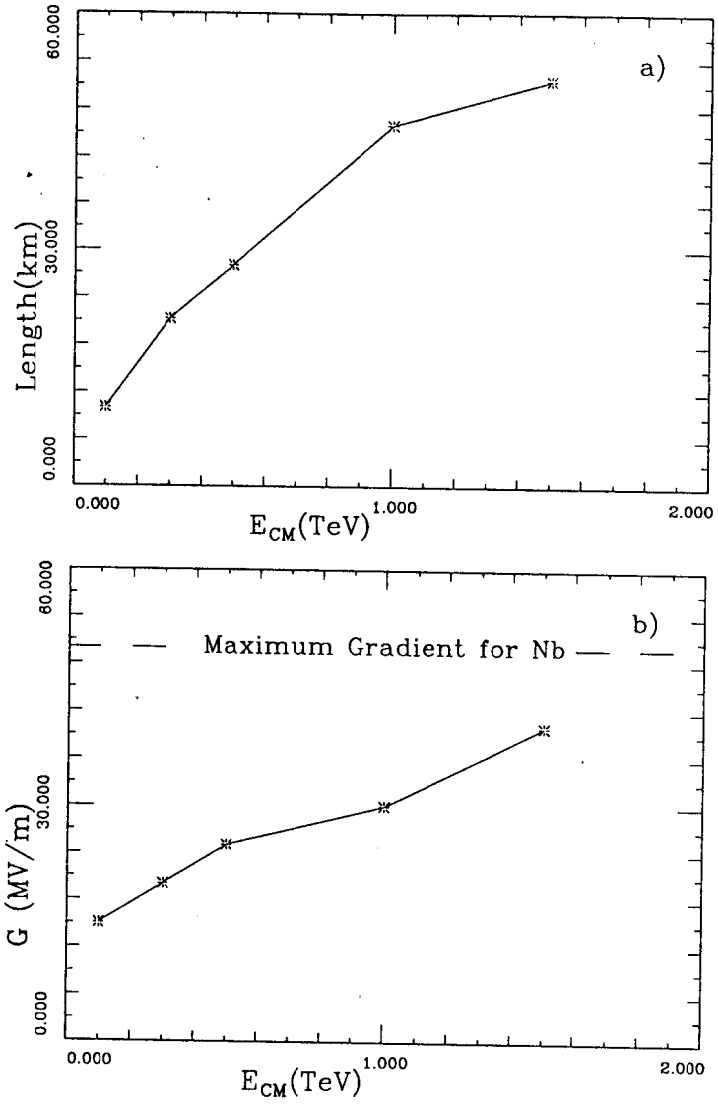

Figure 32: The (a) length and (b) gradient for TESLA from the 1990 Workshop[51].

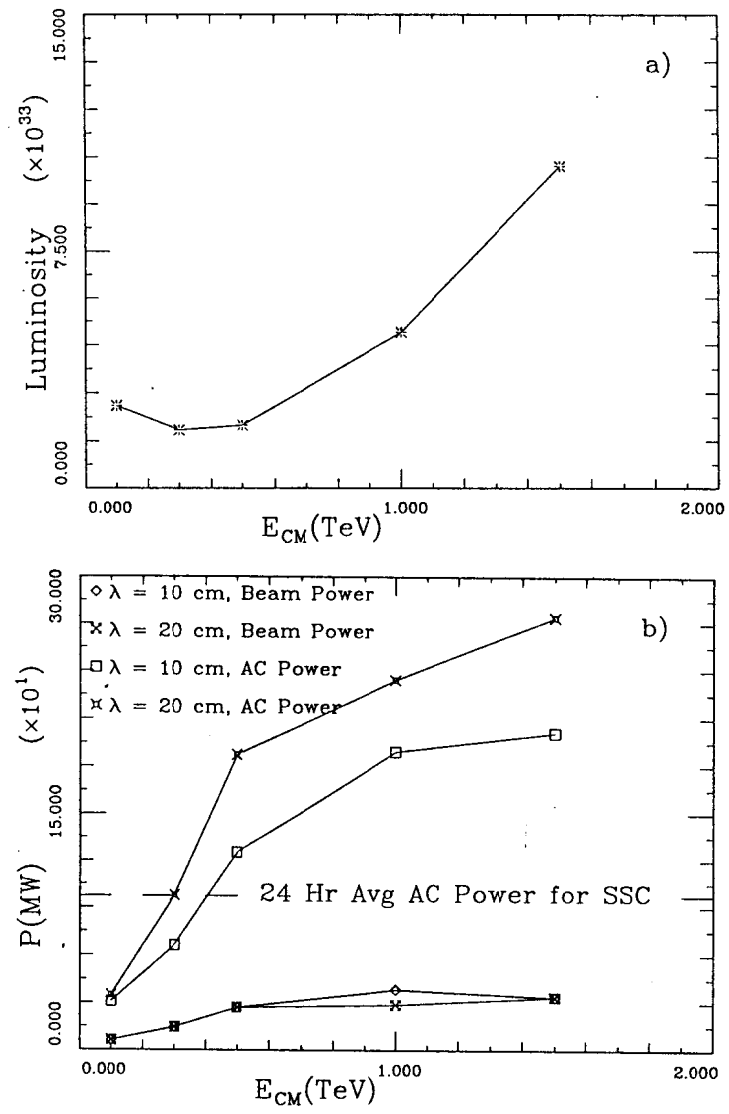

Figure 33: The (a) luminosity and (b) beam power and AC mains power for TESLA from the 1990 Workshop[51].

Critics of superconducting linear colliders express concern about the cost. There are a number of ways to make cost estimates. One is to look at existing systems, but these costs have a large variability and the existing systems are tiny compared to a linear collider. Another is to design to a cost, and $70,000/m is a suggested goal[54]. A Z-factory would cost over $500,000,000 at that rate. Designing to cost may or may not be possible - technology and costs interact. For example, the least expensive way to build cavities is by sputtering Nb onto a copper shell, but copper melts below the temperature needed for the heat treatment that reduces field emission. Based on the experience of high energy physics with the SSC cost where a mature technology is used, my conclusion is that a superconducting linear collider will be expensive but the technology and costs are so uncertain that present cost estimates are meaningless.

3.9 Comparison of Room Temperature and Superconducting Linear Colliders

The TESLA collider in Table III has a collision spot with $\sigma_H = 1\ \mu m$ by $\sigma_V = 100$ nm and a luminosity of $\pounds = 2.1\times10^{33} cm^{-2}s^{-1}$. The beam power, AC power, efficiency, length, and spot size are substantially larger than for a room temperature collider with comparable luminosity. For example, collider J in ref. [46] has $\pounds = 2.5\times10^{33} cm^{-2}s^{-1}$, 2.5 MW of beam power, 70 MW of AC power, $\eta = 3.6\%$, a total length of 6.6 km, $\sigma_H = 440$ nm, and $\sigma_V = 4$ nm. Interestingly, both take about the same AC power, 65 MW, if the RF is pulsed, but no beam accelerated.

The essential difference is that it is possible to have a high beam power with a superconducting collider. The limit on the energy extraction efficiency per bunch (eq. 47) and the cost of making a long enough RF pulse to accelerate a large number of bunches make that much more difficult for a room temperature collider. The higher beam power relaxes the requirements on the final focus, eases the tolerances related to wake fields in the acceleration process and simplifies some aspects of the damping rings. These are substantial advantages, but it isn't clear that they are critical, and there are significant costs: i) the length of the collider, ii) the large amount of AC power needed, and iii) the difficulty of extending the superconducting approach to very high energies.

The best approach can only be decided after the technologies have been developed to a point that experiments testing the critical issues are possible. The advocates of room temperature colliders must demonstrate that they can achieve the spot sizes and tolerances inherent in their approach. The advocates of superconducting colliders must show that the needed performance can be obtained economically. Both groups face exciting challenges!

3.10 Perspective on Superconducting RF

TRISTAN was the first major particle physics application of superconducting RF where it was essential for reaching a center-of-mass energy of over 60 GeV. The application of superconducting RF is becoming wide spread. It is critical for the HERA electron ring, LEP II, and CEBAF, and it offers advantages for some B-factory designs. The progress in superconducting RF is a result of work summarized in Figure 23 that has identified and removed performance limitations. This technology has been transferred to industry, and industrially manufactured cavities with gradients of more than 5 MV/m are available routinely.

High gradient linacs are the frontier of superconducting RF. People are excited about it for linear colliders where it looks attractive for a Z-factory, a Top-factory and possibly even higher energies. Research is focused on improving performance and reducing costs.

High-T_C superconductors have potentially significant advantages. The fundamental gradient limit could be as high as 200 MV/m (vs 50 MV/m in Nb),[55] and a higher operating temperature would increase the Carnot efficiency. Preparation of material for RF applications is a problem, and there does not seem to be strong economic incentive to solve it. As a result the progress to date in applying high-T_C materials to RF is limited.

4. CONCLUDING COMMENTS

Superconductivity and its application to accelerators is becoming increasing important to high energy physics. I have covered some aspects of this enormous topic - aspects that reflect my interests and expertise. Someone else would have used the same title as the starting point for an entirely different set of lectures. I hope that despite the limited coverage the lectures convey a sense of the physics and technology behind particle physics discoveries.

David Larbalestier and Peter Schmüser have written valuable articles about superconductivity and superconducting magnets and have willingly responded to my questions and requests as I prepared these notes. I want to acknowledge Bob Palmer for discussions about his reviews of superconducting magnets (written with A. Tollestrup) and linear colliders. Marvin Weinstein and Dave Coward made some particularly penetrating comments during the Summer Institute that helped me understand this material better. Thanks!

This work was supported by the Department of Energy contract DE-AC03-76SF00515.

5. REFERENCES

1. G. Dugan, private communication.
2. G. Caryotakis, private communication.
3. G. Bachy *et al.*, *Part Accel* **26**, 19 (1990).
4. J. S. McCarthy, B. E. Norum and R. C. York, *Proc of the 12th Int Conf on High-Energy Accel*, 397(1983).
5. H. A. Grunder *et al.*, *Proc of the 1987 IEEE Part Accel Conf*, 13(1987).
6. J. Bardeen, L. N. Cooper, and J. R. Schrieffer, *Phys Rev* **106**, 162 (1957).
   J. Bardeen, L. N. Cooper, and J. R. Schrieffer, *Phys Rev* **108**, 1175 (1957).
7. Charles Kittel, *Introduction to Solid State Physics*, (New York, John Wiley & Sons, 1986).

8. A. C. Rose-Innes and E. H. Roderick, *Introduction to Superconductivity*, (Oxford, Pergamon Press, 1969).
9. F. R Huson *Proc of the 12th Int Conf on High-Energy Accel*, 77(1983).
10. P. M. Morse and H. Feshbach, *Methods in Theoretical Physics*, (New York, McGraw-Hill, 1953), p. 1188.
11. K.-H. Meß and P. Schmüser, *CERN Accel School - Superconductivity in Particle Accelerators*, 87(1989).
12. R. B. Palmer, private communication.
13. R. Palmer and A. V. Tollestrup, *Ann Rev Nucl Part Sci* **34**, 247 (1984).
14. E. Willen *et al.*, *AIP Conf Proc* **153**, 1228 (1987).
P. Dahl, *AIP Conf Proc* **184**, 1327 (1989).
15. J. L. Olsen and C. Palmy, *CERN Accel School - Superconductivity in Particle Accelerators*, 16(1989).
Ph. Lebrun, *CERN Accel School - Superconductivity in Particle Accelerators*, 41(1989).
16. M. N. Wilson, *Superconducting Magnets*, Clarendon Press, Oxford, 1983.
17. *SSC Site Specific Conceptual Design.*
18. *Conceptual Design of the SSC*, (SSC-SR-2020).
19. D. Larbalestier, 1991 IEEE National Particle Accelerator Conference.
20. M. A. Green, *Accelerator Physics Issues for a Superconducting Super Collider* (UM HE 84-1), 126 (1983).
21. H. E. Fisk *et al.*, *Proc of the 1984 Summer Study on the Design and Utilization of the SSC*, 329 (1984).
22. E. D. Courant and H. S. Snyder, *Annals of Physics* **3**, 1 (1958).
23. N. C. Christofilos, unpublished manuscript (1950).
24. M. Hénon, *Quart Appl Math* **3**, 291 (1969).
25. S. G. Peggs and R. Talman, *Ann Rev Nucl Part Sci* **36**, 287 (1986).
26. P. W. Anderson, *Phys Rev Lett* **9**, 309 (1962).
27. P. Schmüser, *Rep Prog Phys* **54** 683 (1991).
28. D. Larbalestier, *Physics Today* **44**, 74 (1991).
29. Matthew Sands, *The Physics of Electron Storage Rings - An Introduction*, SLAC-121 (SLAC, 1970).
30. *LEP Design Report*, CERN-LEP/84-01, (CERN, 1984).
31. H. Lengeler, *CERN Accel School - Superconductivity in Particle Accelerators*, 197(1989).
32. H. Piel, *CERN Accel School - Superconductivity in Particle Accelerators*, 149(1989).
33. J. Matricon and D. St. James, *Phys Lett*, **24A**, 241 (1967).
34. V. Lagomarsino, G. Manuzio, R. Parodi and R. Vaccarone, *IEEE Trans* **MAG-15**, 25 (1979).
35. U. Klein and D. Proch, *Proc of Conf on Future Possibilities for Electron Accelerators*, N1 (1979).
36. H. Padamsee, "Superconducting RF", CLNS 90-1004 (Cornell, 1990).
37. C. Arnaud *et al.*, *Part Accel* **29**, 47 (1990).
38. H. Padamsee in Reference 51.
39. E. Haebel, P. Marchand, J. Tückmantel, CERN/EF/RF 84-2 (CERN, 1984).
40. T. Weiland, CERN/ISR-TH/80-07 (CERN, 1980).
41. *CESR-B Conceptual Design for a B Factory Based on CESR*, CLNS 91-1050.
42. F. Willeke *et al.*, "A B-Factory in the PETRA Tunnel", 1991 IEEE Particle Accelerator Conference.
43. A. N. Dubrovin and A. A. Zholents, "A Combined Symmetric and Asymmetric B-Factory with Monochromatization", 1991 IEEE Particle Accelerator Conference.
44. *Feasibility Study for a B-Meson Factory in the CERN ISR Tunnel*, CERN 90-02, PSI PR-90-08x.
45. F. Takasaki, presentation at *Progress on B-Factories*, June 1991.
46. R. B. Palmer, *Ann Rev of Nuclear Part Science* **40**, 529 (1990).
47. P. B. Wilson, "Linear Accelerators for TeV Colliders", SLAC-PUB-3674 (SLAC, 1985).
48. P. Chen, SLAC-PUB-4822 (SLAC, 1988).
49. K. L. F. Bane, *IEEE Trans Nucl Sci*, **NS-32**, 2389 (1985).
50. R. Sundelin, CLNS-85/709 (Cornell, 1985).
51. H. Padamsee, editor, *Proc of the 1st TESLA Workshop*, CLNS 90/1029 (Cornell, 1990).
52. Reference 51, p 637.
53. Reference 51, pp 165-167.
54. Reference 51, p 384.
55. H. Padamsee *et al.*, CLNS 89/929 (Cornell, 1989).